Published in: *Engineering Structures*, 85C, 234-248.
DOI: http://dx.doi.org/10.1016/j.engstruct.2014.12.033

# Harmonic analysis of measured initial geometric imperfections in large spiral welded carbon steel tubes

Adam J. Sadowski[1], Sjors H.J. van Es[2], Thomas Reinke[3], J. Michael Rotter[4], A.M. (Nol) Gresnigt[5] & Thomas Ummenhofer[6]

## Abstract

Geometric imperfections have long been known to play an important role in determining the buckling resistance of metal cylindrical shells and tubes. Though the effect is more important in thin shells rather than thicker tubular members, it may still have a significant impact on the strength of tubulars where buckling occurs in the plastic range.

Spiral welded carbon steel tubes with *D*/*t* ratios in the approximate range 50 to 150 are often used as primary load-bearing members together with sheet piling in deep retaining walls. A recent European study on such tubes aimed to devise improved and more economical design guidelines for their use. As a central part of this project, a representative selection of 18 tubes was subject to a laser survey to obtain detailed scans of the initial imperfections found on their outer surfaces, in addition to careful wall thickness measurements. The resulting high quality data set is considered to be the first of its kind.

The surface imperfections of the full set of 18 tubes were collectively analysed using a combination of single and double Fourier series to assess the dominant imperfection modes and their amplitudes. It was found that the spiral welding process results in a very unique pattern of surface imperfections which is here characterised algebraically. The systematic peak geometric deviations of the tube surfaces were found to be modest and consistent with the imperfection amplitudes defined by EN 1993-1-6 for this *D*/*t* range.

Published in: *Engineering Structures*, 85C, 234-248.
DOI: http://dx.doi.org/10.1016/j.engstruct.2014.12.033

## Keywords

Spiral-welded tubes, thick tubes, geometric imperfections, harmonic analysis, imperfection characterisation.

[1] Lecturer, Department of Civil and Environmental Engineering, Imperial College London, UK: a.sadowski@imperial.ac.uk

[2] PhD Student, Department of Structural Engineering, Delft University of Technology, The Netherlands: S.H.J.vanEs@tudelft.nl

[3] Research Assistant, Versuchsanstalt für Stahl, Holz und Steine, Karlsruhe Institute of Technology, Germany: T.Reinke@gmx.de

[4] Professor, Institute for Infrastructure and Environment, The University of Edinburgh, UK: m.rotter@ed.ac.uk

[5] Associate Professor, Department of Structural Engineering, Delft University of Technology, The Netherlands: a.m.gresnigt@tudelft.nl

[6] Professor, Versuchsanstalt für Stahl, Holz und Steine, Karlsruhe Institute of Technology, Germany: thomas.ummenhofer@kit.edu

Published in: *Engineering Structures*, 85C, 234-248.
DOI: http://dx.doi.org/10.1016/j.engstruct.2014.12.033

## 1. Introduction

Spiral welded cylindrical carbon steel tubes are often used as piles and with sheet pile walls where they offer a significantly increased resistance against flexure [1]. The practical range of diameter to thickness ratios ($D/t$) of such tubes is approximately 50 to 150. These may be designed either as a 'thin tube' using beam theory and a global stress resultant criterion [2] or as a 'thick shell' using shell theory and a local stress criterion [3]. Unfortunately, the differences in the design philosophy between these two standards have resulted in a substantial and unnecessary discrepancy between the provisions of both standards for tubes in this $D/t$ range.

This discrepancy is the *raison d'être* of the RFCS-funded Combitube project [4], performed in partnership with the Universities of Edinburgh (UK), Delft (Netherlands) and Thessaly (Greece), the Karlsruhe Institute of Technology (Germany), ArcelorMittal (Luxembourg) and BAM Infraconsult (Netherlands) and recently completed in the summer of 2014. The aim of the project is to draw up safe and economical design rules for tubes in bending based on an extensive programme of experimental and numerical studies. A major part of the project consists of the testing of several full-scale specimens under global bending, performed simultaneously at the Delft University of Technology (TU Delft) and the Karlsruhe Institute of Technology (KIT), in each case preceded by detailed laser surveys of the exterior surfaces of these tubes which are the focus of this paper. The resulting very high quality data set of initial geometric imperfections associated with the spiral welding process is believed to be the first of its kind.

## 2. Background to the interpretation of imperfection measurements

This study of the measured imperfections in spiral welded tubulars exploits the numerous studies undertaken since the 1960s to characterise imperfections for accurate prediction of the buckling resistance of shell structures. Full-scale imperfection surveys that mapped the shell surface deviations may be traced to the work of Arbocz, Babcock and Singer [5-9] for the aerospace industry. This early work led to the proposed "Imperfection Data Bank" [10-16] to permit realistic imperfection shapes to be related to the fabrication process. More recently, similar full-scale surveys were made of

aluminium shells for the Ariane space programme [17,18], composite cylinders for aerospace and marine applications [19-22] and spherical LNG storage tanks [23,24].

Surveys of large-scale civil engineering shells are relatively recent, but it was recognised that geometric imperfections found in such shells are significantly different to those in aerospace shells due to the widely different manufacturing processes and difference in scale, making them worthy of study in their own right [25]. Clarke and Rotter [26] may have been the first to survey geometric imperfections in a thin-walled cylindrical steel silo, while Coleman *et al.* [27] and Ding *et al.* [28-30] devised an improved measuring technique for large-scale silos and tanks involving a moving measuring trolley with biaxial degrees of freedom. Together with careful later studies by Berry *et al.* [31-33], Pircher *et al.* [34] and Teng *et al.* [35], it was shown definitively that measured imperfections in most civil engineering shells are dominated by axisymmetric depressions caused by the welding of curved circumferential panels. This contrasted with the asymmetric imperfections typically found in aerospace and laboratory shells which often have longitudinal seams (e.g. [5,8,18]). Previous analytical studies had already established that axisymmetric imperfections generally lead to the most dramatic strength reductions in cylindrical shells (e.g. [36,37]) and computational studies have since confirmed that the imperfections caused by circumferential welding are the most damaging for cylindrical civil engineering shells [33,38,39].

It remains a formidable challenge to produce simplified characterisations of imperfection measurements suitable for use in the design of shell and tubular structures. A powerful method of data reduction practiced by the early aerospace engineers was harmonic analysis, appropriate for full 3D imperfection surveys and simple enough to be programmed on early computers. The result was a complete spectrum of Fourier harmonics which allowed possible critical imperfections to be identified by their relative amplitude and characterised by their wave number (see references by Arbocz and Singer). Though widely used to analyse measured imperfections in civil engineering shells (e.g. [30,35,40-43]), for design purposes the focus has generally shifted towards finding idealised mathematical representations of characteristic imperfections caused by specific manufacturing processes or construction details [38,44-48]. These include the circumferential weld depression

Published in: *Engineering Structures*, 85C, 234-248.
DOI: http://dx.doi.org/10.1016/j.engstruct.2014.12.033

[38], lap-joints [49,50], misfits of curved panels [51,52], local foundation settlement [53], global out-of-roundness [3,54] and local wall flattening [55], amongst many others.

The authors do not know of any previous 3D surveys or characterisations of geometric imperfections in spiral welded cylindrical tubes. This paper presents a detailed summary, harmonic analysis, interpretation and characterisation of 'as measured' patterns of initial geometric imperfections found in sixteen spiral welded and two longitudinally-welded 'control' tubes with $D/t$ ratios ranging from 67 to 119. Though the influence of imperfections is often more dramatic in thin shells that buckle elastically, they may still significantly reduce the strength of thicker tubular members where buckling under global bending occurs in the plastic range. From a structural perspective, the critical terms in the harmonic analysis are usually not those with the largest amplitudes (typically low harmonics), but those whose wavelength is close to that of the critical buckling mode (typically a high harmonic). However, the structural consequences of the imperfections described here is beyond the scope of the paper.

## 3. Experimental procedure for measuring initial surface imperfections

### 3.1 Introduction

This paper explores the initial geometric imperfections in spiral welded tubes based on careful laser surveys performed at TU Delft and KIT. A detailed account of the two different surveying procedures is presented here. The processing and analysis of the data were performed within the 64-bit Matlab R2013a [56] programming environment.

Published in: *Engineering Structures*, 85C, 234-248.
DOI: http://dx.doi.org/10.1016/j.engstruct.2014.12.033

Table 1 – Detailed summary of all surveyed tube specimens (nominal geometry values)

| Tube No. | Steel grade | Diameter $D$ (mm) | Thickness $t$ (mm) | Ratio $D/t$ | Surveyed length $L$ (mm) | Helical angle $\alpha$ (°) | No. of helical turns $n_p$ | No. of circumferential generators | Non-spiral welds present |
|---|---|---|---|---|---|---|---|---|---|
| T1 | X70 | 1067 | 15.9 | 67.1 | 7626 | 29.39 | 4.04 | 16 | Coil† & girth† |
| T2 | X70 | 1067 | 15.9 | 67.1 | 7628 | 29.43 | 4.03 | 16 | |
| T3 | X70 | 1067 | 13.5 | 67.1 | 7630 | 29.43 | 4.04 | 16 | |
| T4 | X70 | 1067 | 15.9 | 67.1 | 7631 | 29.43 | 4.04 | 8 | |
| T5 | X70 | 1067 | 15.9 | 67.1 | 7627 | 29.39 | 4.04 | 16 | Coil† |
| T6 | X60 | 1067 | 9 | 118.6 | 7637 | 22.39 | 5.53 | 8 | |
| T7 | X60 | 1067 | 9 | 118.6 | 7630 | 22.39 | 5.52 | 8 | |
| T8 | X60 | 1067 | 9 | 118.6 | 7630 | 22.45 | 5.51 | 16 | |
| T9 | X60 | 1067 | 9 | 118.6 | 7630 | 22.44 | 5.51 | 8 | |
| T10 | X60 | 1067 | 9 | 118.6 | 7629 | 22.48 | 5.50 | 16 | Coil† & girth† |
| T11 | X60 | 1067 | 9 | 118.6 | 7633 | 22.43 | 5.52 | 8 | Girth† |
| T12 | X60 | 1067 | 9 | 118.6 | 7631 | 22.43 | 5.51 | 16 | Girth† |
| T13 | X52 | 1067 | 13 | 82.1 | 7629 | 29.74 | 4.00 | 16 | Coil† & girth† |
| T14 | X52 | 820 | 11 | 74.6 | 8878 | 35.54 | 4.82 | Continuous | Coil‡ |
| T15 | X52 | 820 | 11 | 74.6 | 10492 | 35.56 | 5.70 | Continuous | Coil† |
| T16 | X52 | 863 | 8.4 | 102.7 | 10518 | 27.87 | 7.34 | Continuous | Girth† |
| T17 | X60 | 1067 | 11 | 97.0 | 7654 | *n/a* | *n/a* | 16 | Longitudinal* |
| T18 | X70 | 1067 | 15 | 71.1 | 7630 | *n/a* | *n/a* | 16 | Longitudinal* |

Note: † - this particular type of weld is near the tube midspan

‡ - this particular type of weld is near the tube edge

* - control specimen, not spiral welded

A total of 16 spiral welded tubes were surveyed for this study together with 2 longitudinally-welded 'control' specimens, summarised in Table 1. Fifteen of these were surveyed at TU Delft (T1 - T13 as well as the two control specimens T17 and T18) while three were surveyed at KIT (T14 - T16). The nominal steel grade of the tubes ranged from X52 or $f_y$ = 355 MPa to X70 or $f_y$ = 450 MPa, representative of such tubes used in practice. A statistical analysis of characterised tensile tests from similar tubes was performed by Sadowski *et al.* [57], offering bounds on post-yield material

properties and suggesting that the spiral welded tubes may be effectively treated as isotropic. Since the forces required to deform the steel sheet from the coil into the helical tubular form depend linearly on the yield stress, one might also suppose that the amplitudes of the imperfections caused by those forces are also linearly related to the yield stress. However, as the spread of steel grades is small it is assumed here that all specimens can be treated as part of the same population for the imperfection assessment. A number of the spiral welded specimens contained either a girth weld (where two segments of spiral welded tube were welded together to form a single specimen), a coil weld (joining the ends of two steel coils as the tube is spirally rolled) or both. Each of these welds leads to an additional systematic imperfection pattern caused by the manufacturing process.

### 3.2 Surveying procedure at TU Delft

The measurements of the initial surface imperfections of the fifteen specimens at TU Delft were performed with a Sensopart FT50 RLA-40-F [58] laser scanner mounted on a specially designed mobile trolley. The specimen was placed on two stiff supports while the trolley slowly travelled along the designated survey length of the tube (approximately 7630 mm) and scanned the underside of the specimen (Fig. 1). The laser scanner was also used to scan along a trough containing an opaque liquid positioned parallel to the specimen. The measurements of the tube surface were then related to the flat surface of the liquid to provide a truly horizontal reference. The specimen was then successively rotated about its axis through a fixed increment and the scan repeated. A first group of specimens were scanned using only 8 generators (angular increment = 45°), but all others used 16 generators (increment = 22.5°) to detect more detail. The meridional resolution of all scans was very high with approximately one observation per mm. The position of the trolley was identified from the total rotation of one of the wheels using an angular displacement transducer, and the net outer surface deviation was thus expressed in terms of the relative position of the trolley. A floating average filter was applied to smooth the resulting curves. An extended account of the experimental programme and initial imperfection processing carried out at TU Delft may be found in van Es *et al.* [59].

Published in: *Engineering Structures*, 85C, 234-248.
DOI: http://dx.doi.org/10.1016/j.engstruct.2014.12.033

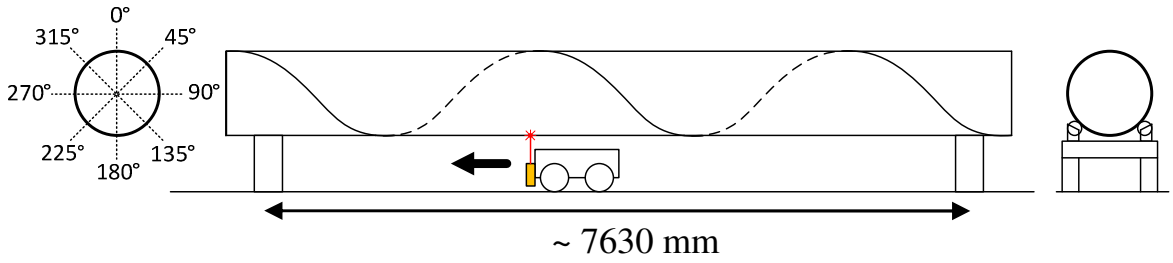


Fig. 1 – Schematic of the laser scanning trolley at TU Delft and the meridional generators (illustrated at 45°)

A number of the specimens surveyed at TU Delft were additionally also subject to a series of detailed wall thickness measurements at different locations (Fig. 2a). Sets of measurements were taken at 45° circumferential intervals around 5 stations at 1500 mm separations symmetric about the midspan (Stations 1 - 5). Additionally, wall thickness measurements were taken transversely to the coil in spiral welded specimens T1 - T3 and T5 - T13 (Trans 1 & 2). The mean of the measured values along each position shows that the 'true' tube thickness is generally very close to the nominal value (Fig. 2b). More importantly, the wall thickness measurements exhibit mean coefficients of variation of at most only 0.85% (CV = $\mu/\sigma$ where $\mu$ and $\sigma$ are the mean and standard deviations respectively) suggesting a very well-defined mean value with little scatter across the full range of available specimens (Fig. 2c). Since TU Delft tested the majority of the tubes (83%), it may be assumed for practical purposes that the spiral welded tubes of comparable quality in this $D/t$ range effectively have a constant wall thickness and thus the imperfection data corresponding to the outer tube surface may be taken to apply to the midsurface for the purposes of characterisation. Also shown in Figs 2b & 2c are 95% Confidence Interval bars around the sample mean values (calculated as ±1.96SE where SE is the standard error given by $\sigma/\sqrt{n}$ where $n$ = 15 (Stations 1 - 5) and $n$ = 12 (Trans 1 & 2) is the number of specimens) denoting with 95% confidence the range in which the 'true' population mean may be expected to be found [60]. This interpretation of error bars is used throughout this study.

Published in: *Engineering Structures*, 85C, 234-248.
DOI: http://dx.doi.org/10.1016/j.engstruct.2014.12.033

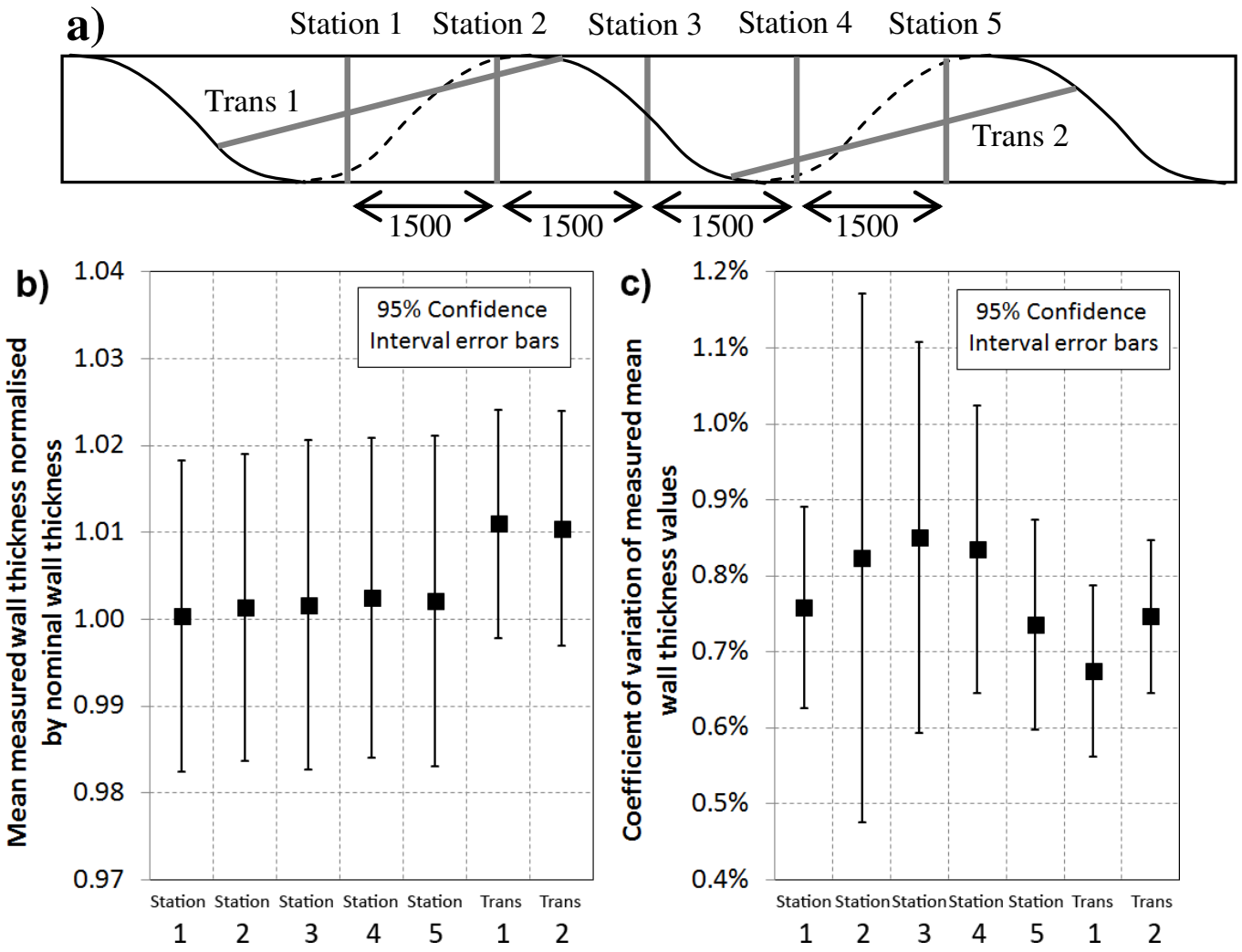


Fig. 2 – Illustration of wall thickness measurements: a) sampling locations; b) mean normalised wall thicknesses and c) coefficients of variation (shown with 95% Confidence Interval error bars)

### 3.3 Surveying procedure at KIT

The measurements of the initial surface imperfections of the three tube specimens at KIT were performed in a different manner using a Leica ScanStation C10 [61]. The specimens were again positioned on two stiff supports while the scanning device was installed at a distance of approximately 5 metres away from specimen at the level of the centreline (Fig. 3). In this position, a quarter of the surface area of the specimen could be scanned after which the specimen was turned by 90° and the process was performed again, four times in total. Carefully chosen reference points were then used to merge the four surveys into a single data set, a task requiring substantial computing power which was performed by a commercial third party company. The measurements

Published in: *Engineering Structures*, 85C, 234-248.
DOI: http://dx.doi.org/10.1016/j.engstruct.2014.12.033

of each specimen resulted in at least 10 million sampling points of the surface, corresponding to a very high sampling point density of approximately 35 points/cm$^2$ and at an average point distance of approximately 1.7 mm in both meridional and circumferential directions.


Fig. 3 – Illustration of the surveying setup at KIT

## 4. Data processing with Matlab

The measurement technique and pre-processing implemented at TU Delft resulted in data that was already in the form of net geometric deviations from the shell midsurface and no further action was necessary at this stage. However, the survey data obtained by KIT was in the form of 3D Cartesian coordinates of the exterior surface of the shell and it was necessary to determine the position of the 'perfect' cylinder relative to which the net deviations may be calculated. This 'best-fit' cylinder was found by means of a least squares adjustment using the equations presented in Teng *et al.* [35], though the method may be traced back to the concept of the 'mean' cylinder of Coppa [62] and the

Published in: *Engineering Structures*, 85C, 234-248.
DOI: http://dx.doi.org/10.1016/j.engstruct.2014.12.033

GALCIT electronic system at Stanford University in 1968 and later at the Technion in Haifa [16]. The procedure removes rigid body displacements and rotations of the shell with respect to the scanning system and provides an imaginary cylindrical reference surface for the extraction of 'net' initial geometric imperfections. It has been applied with great success in numerous studies of this nature (e.g. [5,8,19-22,30,35]).

Although every published harmonic analysis in this field employs a full-wave general Fourier series (FWG) to represent the circumferential variation of the imperfection data, there appears to be a significant difference of opinion on the most appropriate choice of Fourier series to model the variation along the meridional axis of the cylinder [63]. A half-wave meridional sine series (HWS) was used by [9,18-22,64-67] while a half-wave meridional cosine series (HWC) was, by itself, only used by [35]. Both forms were used in [5,8] as well as in the Imperfection Data Bank [11], while the meridional FWG was employed by [5,30]. The original motivation for using a half-wave series was that the measured imperfections could be expressed in terms of fewer harmonics, an important consideration when computing power was limited. A HWS was the preferred choice for laboratory-made cylinders with rigid end rings which easily satisfied conditions of zero end displacement, but this justification is no longer valid for civil engineering shells which undergo non-zero displacement at either end. Further, since the resolution of the present survey data was exceptionally high meridionally (several thousand data points) and computational power is now abundant, it was not considered necessary to economise on Fourier terms along any dimension. The following full double Fourier series was therefore adopted:

$$w(z,\theta)=\sum_{m=0}^{M}\sum_{n=0}^{N}\left\{\begin{array}{l}\sin\left(2\pi\dfrac{mz}{L}\right)\left[A_{mn}\cos(n\theta)+B_{mn}\sin(n\theta)\right]\\+\cos\left(2\pi\dfrac{mz}{L}\right)\left[C_{mn}\cos(n\theta)+D_{mn}\sin(n\theta)\right]\end{array}\right\} \quad (1)$$

where $z$ and $\theta$ are the meridional and circumferential coordinates respectively, $m$ and $n$ are the meridional and circumferential mode numbers up to a maximum of $M$ and $N$ respectively, and $L$ is the surveyed length of the cylinder. The Fourier coefficients $A_{mn}$, $B_{mn}$, $C_{mn}$ and $D_{mn}$ may be estimated numerically using the trapezoid rule (for which expressions are written out in full in Ding *et al.* [30]). It may be shown that the modal amplitude $\Delta_{mn}$ is given by:

Published in: *Engineering Structures*, 85C, 234-248.
DOI: http://dx.doi.org/10.1016/j.engstruct.2014.12.033

$$\Delta_{mn} = \sqrt{A_{mn}^2 + B_{mn}^2 + C_{mn}^2 + D_{mn}^2} \quad (2)$$

The application of the 'best-fit cylinder' procedure led to a complete data set that was now fully in the appropriate 'net deviation' format. However, for practical reasons associated with the surveying procedure, the $z$-$\theta$ coordinates of each discrete sampling point did not correspond to a uniformly-spaced grid. The data set could therefore not yet be subject to a traditional Fourier series decomposition according to Eq. 1 as this would not be able to accurately represent the measured discrete imperfections. The reasons for this are described in detail by Lin and Teng [68] who also propose an iterative 1D Fourier decomposition method which overcomes this problem by incrementally refining the Fourier coefficients to minimise a global error criterion. However, it was felt that this procedure would be unnecessarily complicated in the present case where a 2D Fourier series characterisation is desired and where the dataset contains tens of thousands of data points arranged in non-uniformly sized vectors. A simpler solution was to employ the powerful Matlab *griddata* command to map the non-uniform 2D sampling grid onto a uniform one using local 2D surface spline interpolation. This had the dual advantage of enabling the straightforward application of a traditional 2D Fourier series decomposition (Eq. 1) whilst also storing the dataset in computational arrays of uniform dimensions ideally suited for analysis and visualisation.

Published in: *Engineering Structures*, 85C, 234-248.
DOI: http://dx.doi.org/10.1016/j.engstruct.2014.12.033

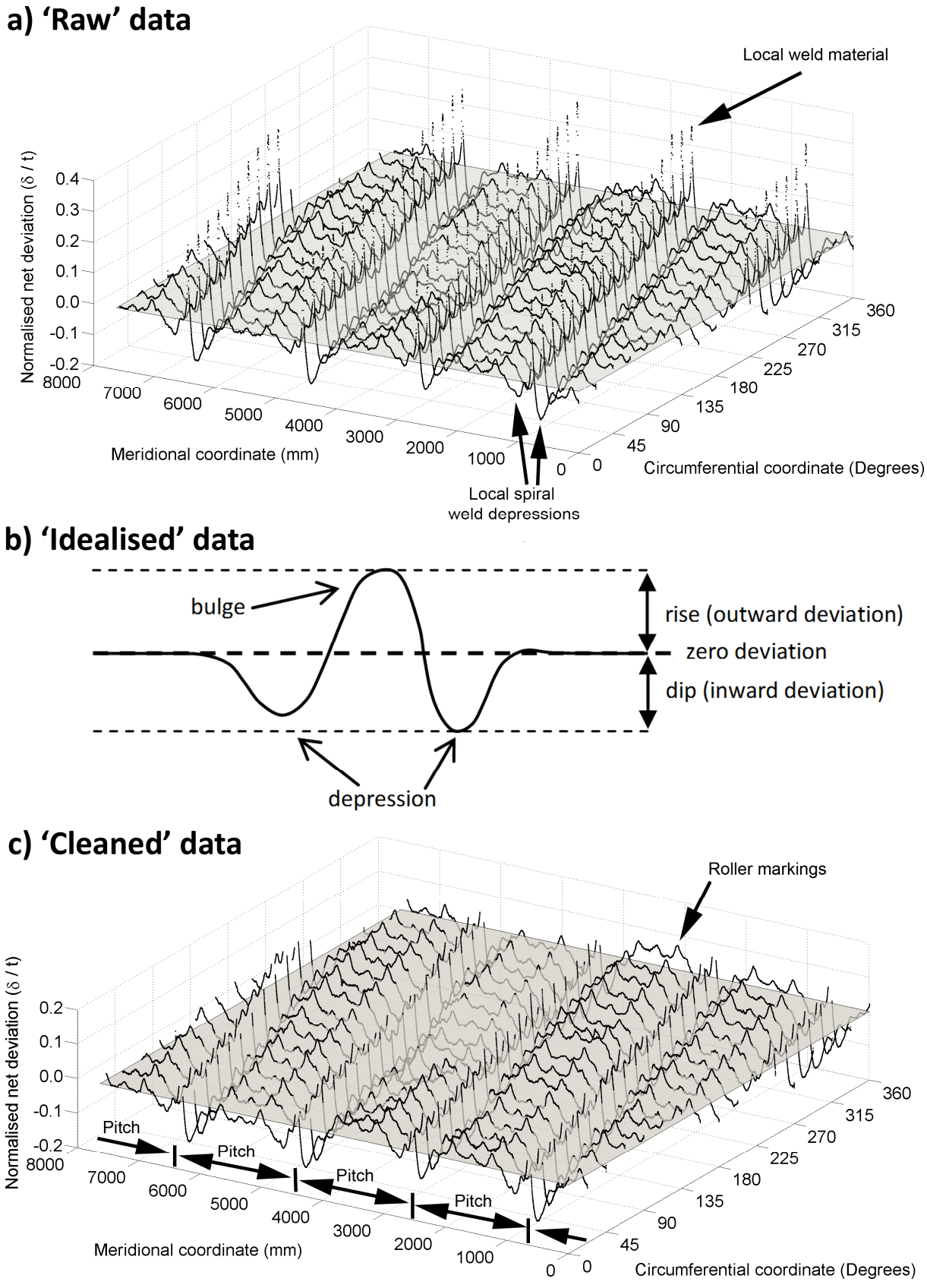


Fig. 4 – Initial 'cleaning' of the net deviation data, illustrated for specimen T2 (the grey plane represents the hypothetical 'perfect' tube surface with zero net deviations)

Published in: *Engineering Structures*, 85C, 234-248.
DOI: http://dx.doi.org/10.1016/j.engstruct.2014.12.033

## 5. Global overview of the specimens

The 'raw' measured net deviation data was first assessed visually on a 3D scatter plot in terms of the coordinates $z$-$\theta$, shown for a typical spiral welded tube in Fig. 4a (specimen T2). The spiral weld appears as a distinct feature that migrates around the circumference following a constant helical angle of inclination $\alpha$ to the diametral plane, repeats itself at the periodic boundary at $\theta = 0°$ and 360° and is separated along every meridian by a constant distance called the 'pitch'. At each spiral weld, the outer surface of the tube appears to exhibit a bulge (outward deviation or 'rise') flanked by two depressions (inward deviation or 'dip'), one usually slightly deeper than the other (shown in an idealised manner in Fig. 4b). The measurements in the vicinity of the bulges contain contributions from the local weld material which was recorded by the laser scan but which are not strictly a part of the characteristic geometric imperfections of the tube. The net deviations were thus carefully processed further to remove the measurements associated with the weld material, and the resulting 'cleaned' net deviation data (Fig. 4c) may be thought of as a reasonably accurate representation of the outer surface of the tube specimen and, by virtue of the approximately constant wall thickness (Fig. 2), of its midsurface. Also visible along each meridional generator are systematic local bumps between the welds which appear to correspond to marks left by the cold rolling process during manufacture [58].

The 'cleaned' imperfection data was inspected to obtain approximate peak outward and inward deviations of the tube outer surface (shown normalised by the wall thickness of the respective specimen in Fig. 5a) that are unaffected by the local weld material. The arithmetic mean of the outward peak deviations was found to be 0.29$t$ with a CV of 53% across all of the specimens, while the mean of the inward peak deviations was found to be 0.41$t$ with a CV of 72%. Three notable outliers appear to be specimens T8, T16 and T17 which exhibit quite large peak inward deviations of 0.60$t$, 0.88$t$ and 1.31$t$ respectively due to the presence of quite severe local indentations most likely caused by accidental impact (Fig. 6). Such dents are not representative of any manufacturing process and when the regions containing these imperfections are removed from the assessment of these tubes the mean inward deviation drops to 0.32$t$ with a considerably smaller CV of 43% (Fig. 5b). These local dents or 'dimples' are already covered by detailed tolerance provisions in fabrication standards such as EN 1090-2 [69] and EN

Published in: *Engineering Structures*, 85C, 234-248.
DOI: http://dx.doi.org/10.1016/j.engstruct.2014.12.033

10219-2 [70] or in the metal shells standard EN 1993-1-6 [3] and require no further characterisation.

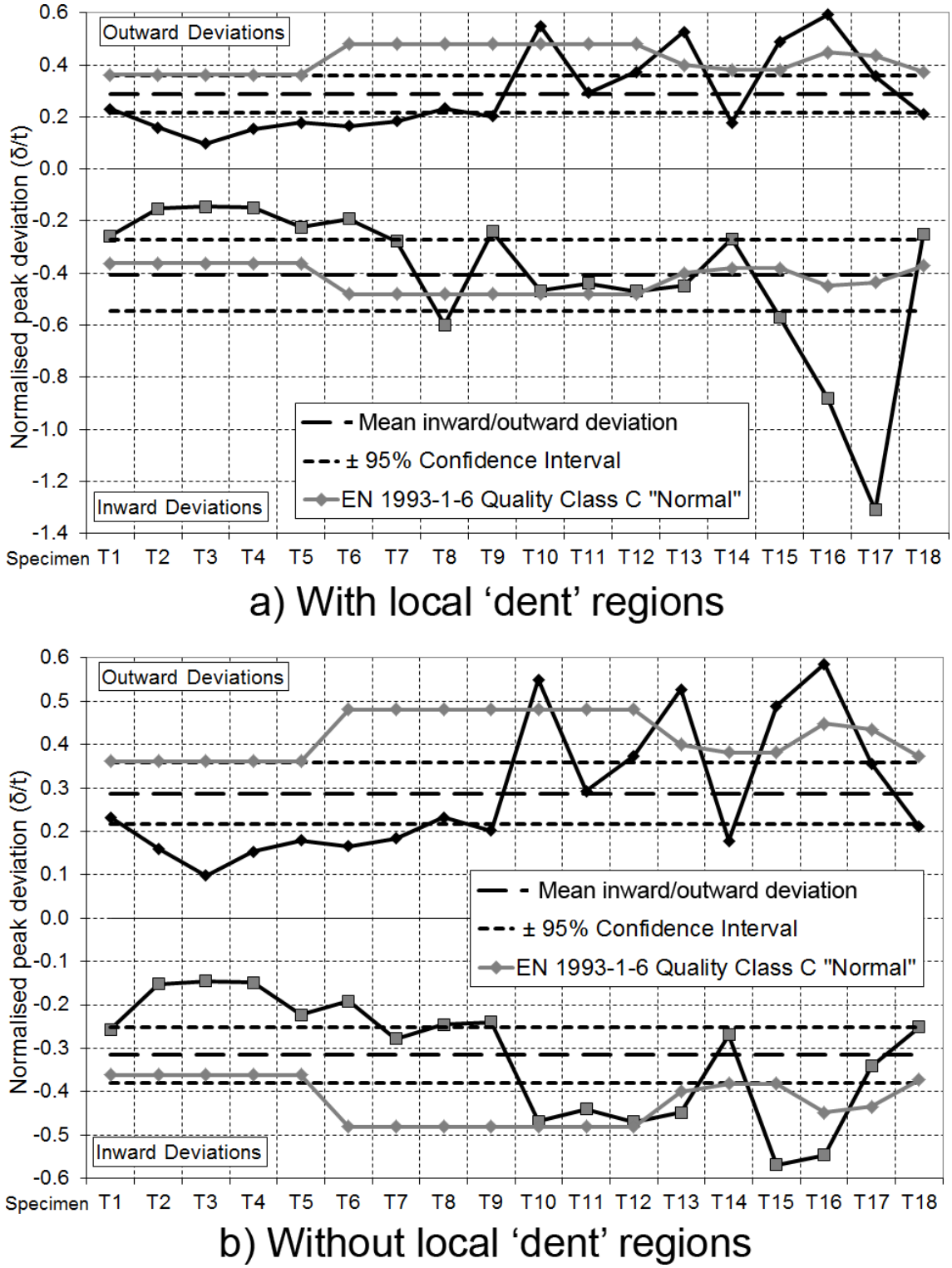


Fig. 5 – Peak filtered outward and inward deviations for each specimen (with and without 'dent' regions), together with mean values and 95% Confidence Interval bands

Published in: *Engineering Structures*, 85C, 234-248.
DOI: http://dx.doi.org/10.1016/j.engstruct.2014.12.033

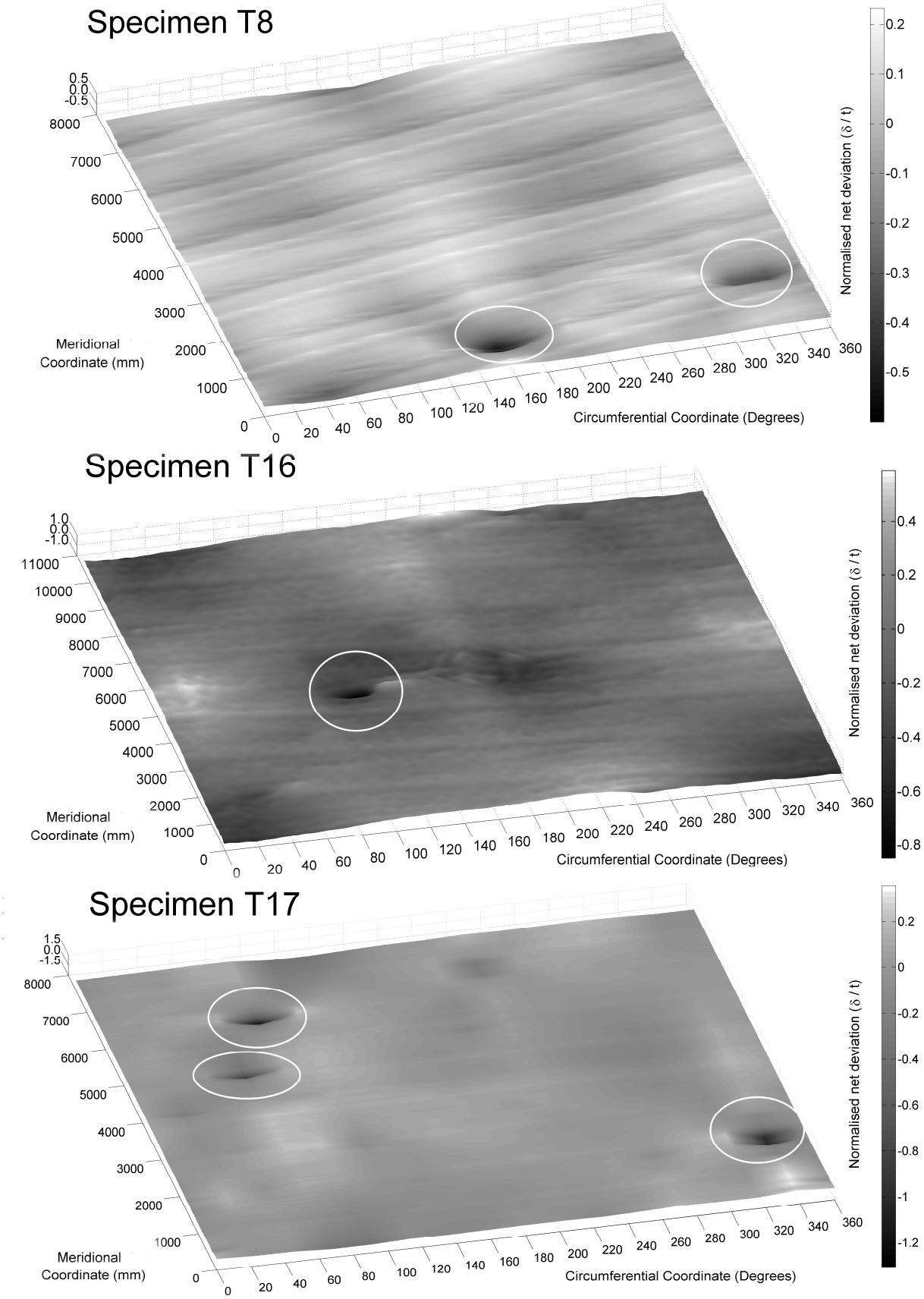


Fig. 6 – Local indentations (circled) found in specimens T8, T16 and T17

Published in: *Engineering Structures*, 85C, 234-248.
DOI: http://dx.doi.org/10.1016/j.engstruct.2014.12.033

The 95% Confidence Interval bands around the sample mean values ($n$ = 18) are narrow suggesting well-defined mean values of inward and outward deviations. The orders of magnitude of the peak inward and outward filtered deviations are consistent with expected imperfection amplitudes for tubes with such $D/t$ ratios and may be seen to generally fall within the bounds of the characteristic imperfection amplitude $\Delta w_k/t$ for the lowest Fabrication Tolerance Quality Class C 'Normal' of EN 1993-1-6 [3]. Lastly, the two control specimens T17 and T18 exhibit peak deviations that are also within the 95% Confidence Intervals around the respective global means, suggesting that tubes in this $D/t$ range that are manufactured by continuous spiral welding do not exhibit imperfections that are of a different order of magnitude than 'traditional' longitudinally-welded tubes. Lastly, it is remarkable that the specimens surveyed at TU Delft (T1 to T13, T17 and T18) do not exhibit significantly different results to those surveyed at KIT (T14 to T16), strongly suggesting that both methods of measurement are consistent.

## 6. Harmonic analysis in the cylindrical coordinate system

The net deviation data for each of the 18 specimens was subsequently put through a full two-dimensional Fourier series decomposition (Eq. 1) using the explicit formulae for the harmonic coefficients $A_{mn}$ to $D_{mn}$ published in Ding *et al.* [30]. The maximum number of harmonics that may be extracted along any particular direction is limited to being *less* than ½($p$ – 1) where $p$ is the number of sampling points along that direction [68]. The meridional resolution of each survey was sufficiently high (several thousand sampling points along each meridional generator) that for practical purposes there was no limitation on the number of meridional harmonics that could be extracted. However, the surveys carried out at TU Delft used between 8 and 16 discrete meridional generators equally spaced around the circumference (respectively giving $p$ = 9 and 17 sampling points due to the period boundary condition at $\theta$ = 0° and 360°), meaning that the maximum number of meaningful circumferential harmonics that could be extracted was 3 and 7 respectively. The limit of 3 harmonics affected only 5 out of the 16 spiral welded specimens. The specimens surveyed at KIT were not limited in this way because the circumferential resolution there was so high as to effectively be continuous.

Published in: *Engineering Structures*, 85C, 234-248.
DOI: http://dx.doi.org/10.1016/j.engstruct.2014.12.033

The very numerous harmonic coefficients $A_{mn}$ to $D_{mn}$ computed in this manner were combined into a single aggregate modal amplitude $\Delta_{mn}$ (Eq. 2) to greatly reduce the number of individual coefficients that needed to be considered and visualised. The distributions of $\Delta_{mn}$ for each specimen (a type of 2D 'harmonic spectrum') are best illustrated on a contour plot in terms of the meridional and circumferential mode numbers $m$ and $n$ respectively, a selection of which is shown in Fig. 7 for three spiral welded specimens (T2, T11 and T14) together with one longitudinally-welded control specimen (T17). The data points of $\Delta_{mn}$ are defined only at integer values of $m$ and $n$, with contours in-between being artificially generated by the plotting algorithm of Matlab. Modes with $m$ = 1 represent those with a 'bow' or 'column' imperfection, while modes with $n$ = 0, 1 and 2 represent axisymmetric bulging or contraction, rigid cross-section displacement and ovalisation respectively. A close examination of the full set of 2D harmonic spectra allows two very distinct groups of harmonics exhibiting peaks in $\Delta_{mn}$ amplitudes to be identified.

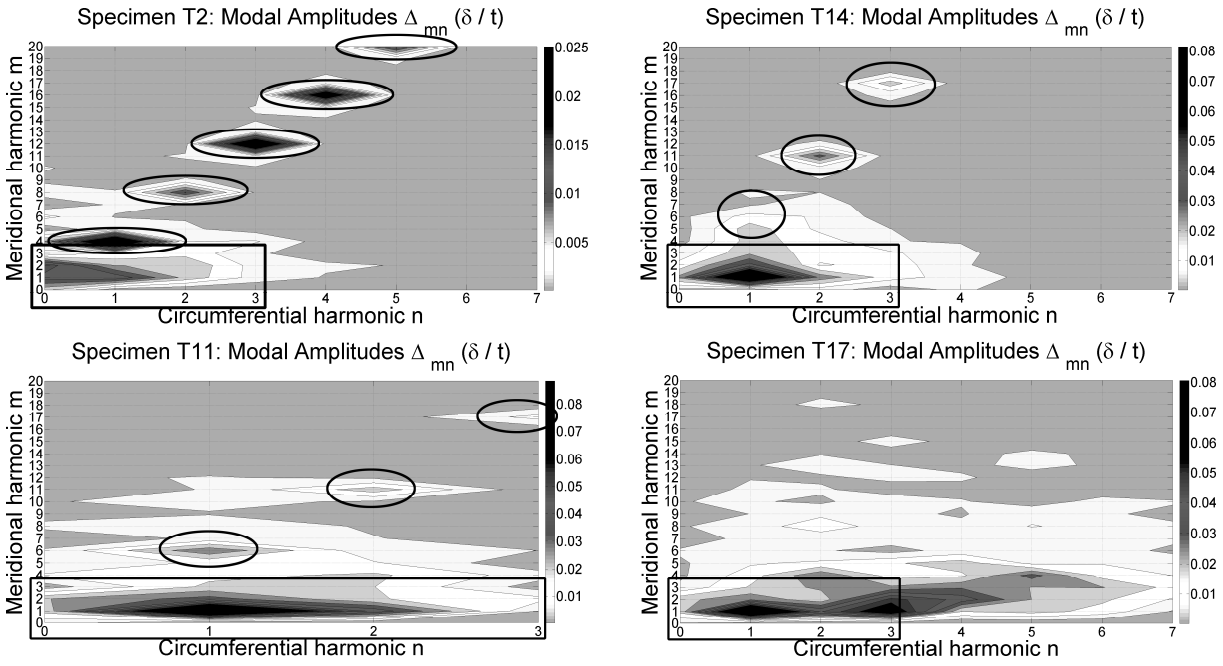


Fig. 7 – 2D harmonic spectra showing normalised modal amplitudes $\Delta_{mn}$ ($\delta/t$) for three spiral welded specimens (T2, T11 and T14) and one longitudinally-welded specimen (T17): the meaning of the circles and squares is explained in the text

The first group encompasses the 'low' harmonics with $m$ and $n$ up to approximately 3 and relate to sagging, misalignment, out-of-roundness and ovalisation imperfections

Published in: *Engineering Structures*, 85C, 234-248.
DOI: http://dx.doi.org/10.1016/j.engstruct.2014.12.033

typically found in any simply-supported tube or cylinder (annotated with a rectangle in Fig. 7; see also references in the literature review). Different specimens exhibit high $\Delta_{mn}$ amplitudes for varying *m*-*n* pairs in this modal range, but the pattern persists across all of the specimens including the two longitudinally-welded controls T16 and T17, indicating that these harmonics are not a characteristic of the spiral welding process. The mean values of $\Delta_{mn}$ for $n \in [0,3]$ and $m \in [0,3]$ across the full range of specimens suggest that even the largest 'bow' ($m = 1$; $n = 1$) and 'ovalisation' ($m = 1$; $n = 2$) harmonics have very modest mean imperfection amplitudes of approximately $0.09t$ (CV = 91%) and $0.04t$ (CV = 61%) respectively (Fig. 8), with all other low harmonics exhibiting significantly smaller amplitudes. The 95% Confidence Intervals are additionally rather narrow (with the exception of $m = n = 1$) suggesting well-defined mean values. These 'low' harmonics are easily characterised by simple trigonometric functions and are currently well described by out-of-roundness and ovalisation tolerance requirements in EN 1993-1-6 [3], which the magnitudes of the deviations presented here satisfy for at least Fabrication Tolerance Quality Class C.

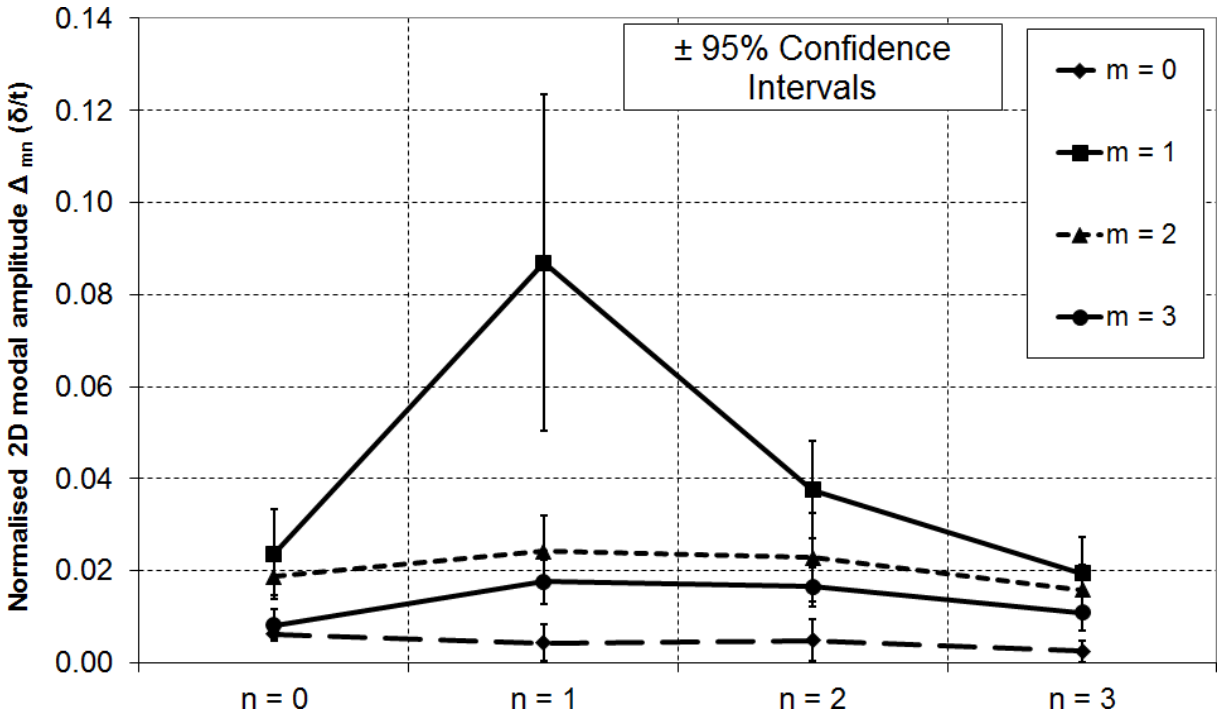


Fig. 8 – Normalised modal amplitudes $\Delta_{mn}$ ($\delta/t$) for $n \in [0,3]$ and $m \in [0,3]$ together with 95% Confidence Interval error bars (calculated on the basis of all harmonic spectra from all 18 specimens)

Published in: *Engineering Structures*, 85C, 234-248.
DOI: http://dx.doi.org/10.1016/j.engstruct.2014.12.033

The second group consists of amplitude peaks occurring approximately at modal pairs $(m,n) \approx ([n \times n_p],n)$, where [] = *round*() denotes rounding to the nearest integer and $n_p$ is the number of helical turns along the surveyed tube length (Table 1). These 'helical' harmonics (circled in Fig. 7) are not present in the control specimens T16 and T17 and therefore relate specifically to the spiral welding process. Though the scatter in these is considerable (Fig. 9), the highest mean amplitude occurs for $n = 1$ (the 'bow' imperfection) with $0.047t$ (CV = 149%) and decays rapidly with increasing $n$ (as does the scatter). It will become evident in what follows that these helical harmonics play a key role in the development of an algebraic characterisation of the spiral weld imperfection which does not appear to have yet been performed in any known published study.

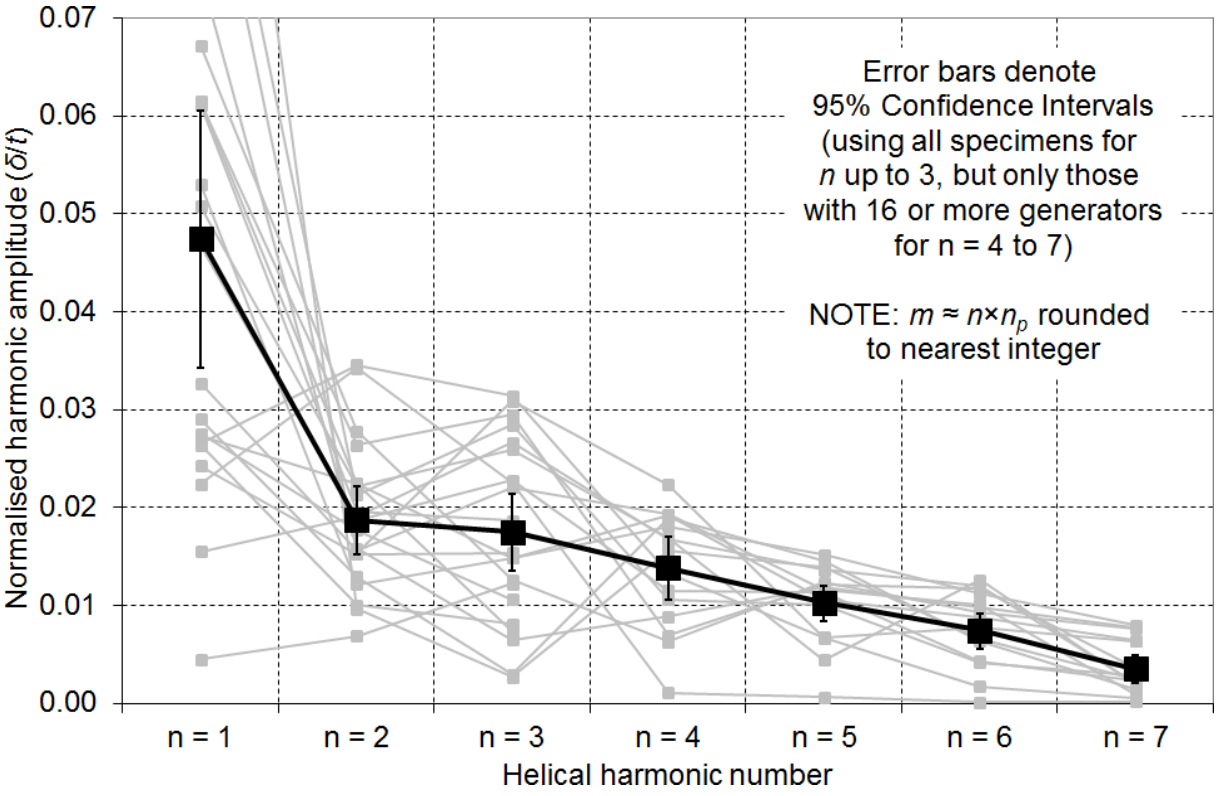


Fig. 9 – Normalised modal amplitudes $\Delta_{mn}$ $(\delta/t)$ for the 'helical' harmonics with $(m,n) \approx ([n \times n_p],n)$ where $n \in [1,7]$: the mean value and 95% Confidence Interval error bars are shown in black while actual values are illustrated in grey

Published in: *Engineering Structures*, 85C, 234-248.
DOI: http://dx.doi.org/10.1016/j.engstruct.2014.12.033

Current descriptions of continuous circumferential welds originate from studies of thin cylindrical shells such as silos and tanks ($D/t$ >1000) which are usually constructed by welding together individual curved panels or strakes of sheet metal. The completed structures exhibit rolling anticlastic bending and thermal-induced shrinkage at the weld locations which lead to approximately axisymmetric and quite well-defined 'depressions' that may be distinctly different from those found in spiral welded tubes with $D/t$ from 50 to 150. These axisymmetric imperfections have been modelled and characterised with some success by [34,38,51,52,71-73] and others. The Type 'A' weld depression of Rotter and Teng [38] in particular (Eq. 3) has been adopted in numerical parametric studies [39,74] and is widely considered as a particularly damaging imperfection for thin cylindrical shells under uniform axial compression and global bending. Indeed, Pircher *et al.* [34] conducted a survey of alternative characterisations of such weld-induced circumferential imperfections, each one of which exhibits geometrically very similar features, and used least-squares curve fitting to show that a characterisation similar to Eq. 3 offers a remarkably good approximation to measured wall-profiles of thin cylindrical welded silos and tanks.

$$w(z) = \delta e^{-\pi|z-z_w|/\lambda}\left(\cos\frac{\pi}{\lambda}|z-z_w| + \sin\frac{\pi}{\lambda}|z-z_w|\right) \tag{3}$$

where $\lambda = \dfrac{\pi\sqrt{rt}}{\sqrt[4]{3\left(1-\nu^2\right)}}$ is the linear meridional bending half-wavelength (4)

and $z_w$ is the meridional location of the centre of a girth weld.

The axisymmetric components of the surface deviations of specimens containing girth welds (T1, T10-T13 and T16) were thus extracted, normalised by the wall thickness and expressed in terms of the meridional coordinate $z$ normalised by the linear meridional bending half wavelength $\lambda$ (Eq. 4). Illustrated in Fig. 10a with the approximate centre of each girth weld centred at $z/\lambda = 0$ (assumed to be the base of each depression), it is clear that there exists a distinct misalignment of the tube components at the location of the girth weld. An estimate of this local misalignment or 'joint eccentricity' $e_a$ was obtained by summing the absolute values of the mean axisymmetric deviations to within 5λ on either side of the joint for each specimen. These eccentricities were found to satisfy at least the relevant EN 1993-1-6 [3] tolerance requirements for Fabrication Tolerance Quality Class C (Table 2).

Published in: *Engineering Structures*, 85C, 234-248.
DOI: http://dx.doi.org/10.1016/j.engstruct.2014.12.033

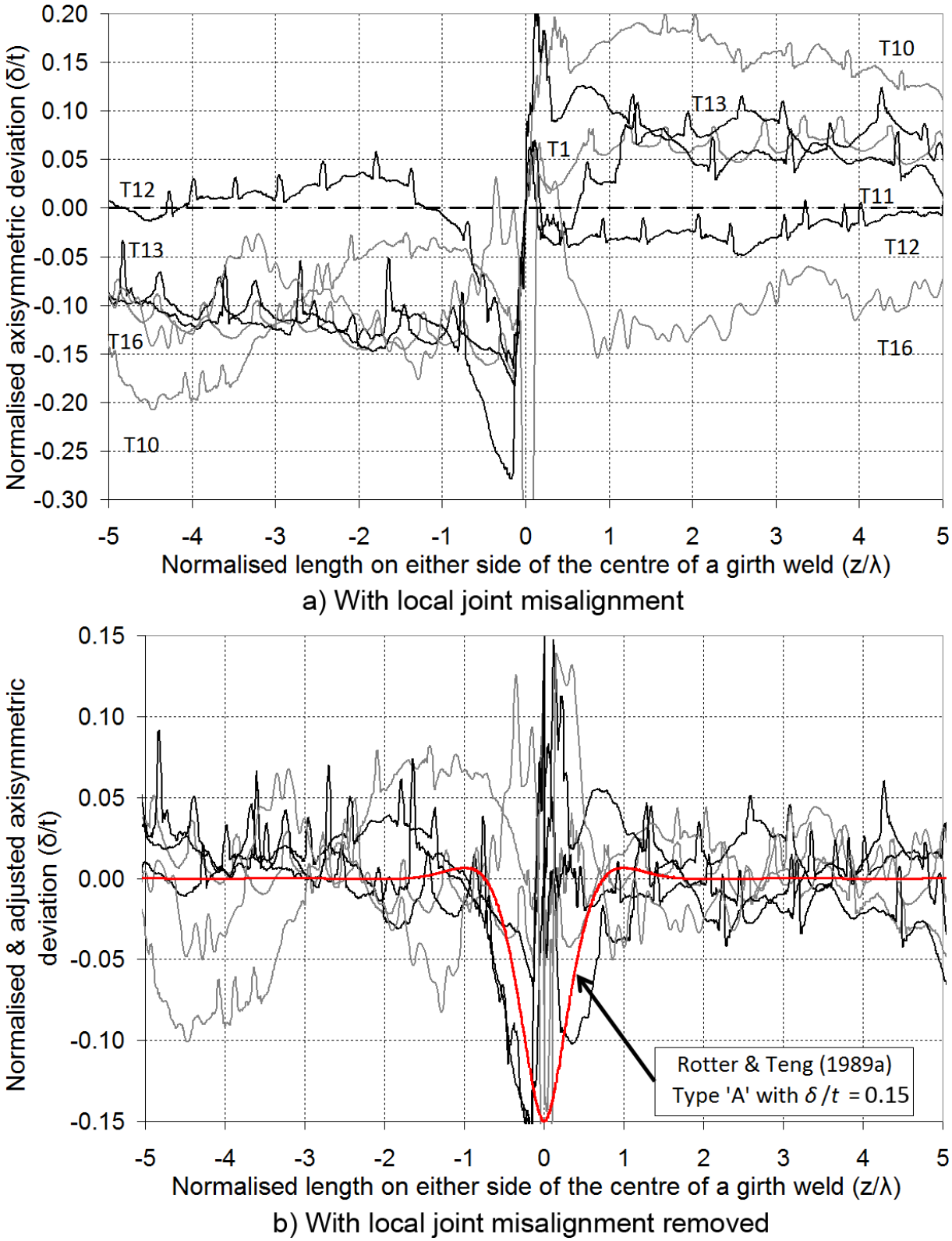


Fig. 10 – Extraction of the axisymmetric component of the measured surface deviations in the vicinity of the girth weld imperfections as well as joint misalignment for six tube specimens

Published in: *Engineering Structures*, 85C, 234-248.
DOI: http://dx.doi.org/10.1016/j.engstruct.2014.12.033

Table 2 – Summary of accidental joint eccentricities and comparison with EN 1993-1-6 [3] tolerance requirements for Fabrication Tolerance Quality (FTQ) Class C

| Parameter | T1 | T10 | T11 | T12 | T13 | T16 | Mean | CV (%) | FTQ Class C |
|---|---|---|---|---|---|---|---|---|---|
| $e_a$ (mm) | 2.95 | 2.35 | 2.37 | 1.76 | 0.21 | 1.66 | 1.89 | 50.2 | 4 |
| $U_e$ ($e_a/t$) | 0.19 | 0.18 | 0.26 | 0.20 | 0.02 | 0.20 | 0.17 | 45.8 | 0.3 |

The axisymmetric deviations were subsequently adjusted to remove the estimated misalignments on either side of the girth weld. The resulting profiles (Fig. 10b) bear a remarkable resemblance to the predicted shape of the Type 'A' weld depression (Eq. 3), shown for an illustratory imperfection amplitude of 0.13*t*, which had originally been developed with significantly thinner cylindrical shells in mind. This algebraic form is thus likely to be a reasonably realistic and highly convenient approximation, particularly for numerical implementation, and may be expected to be conservative across the full practical range of *D*/*t* ratios.

## 7. Harmonic analysis of specimens in the plane of the coil

A harmonic analysis of the imperfection surveys in the cylindrical coordinate system can only yield so much useful information, primarily because the main geometric features of the spiral imperfections are defined in a different plane. A recent study by Sadowski and Rotter [75] devised a mathematical transformation that, in the present context, allows the sampling points to be mapped conformally from the global cylindrical *x*-*y*-*z* 3D space onto the local 'helical' $\chi$-$\eta$ 2D plane of the coil in which the imperfections are significantly easier to visualise and analyse (Fig. 11; $\chi$ and $\eta$ are curvilinear coordinates parallel and transverse to the coil respectively). The original transformation was:

$$x(\chi,\eta) = r(\chi,\eta)\cos\left[\theta(\chi,\eta)\right] \tag{5}$$

$$y(\chi,\eta) = r(\chi,\eta)\sin\left[\theta(\chi,\eta)\right] \tag{6}$$

$$z(\chi,\eta) = \eta\sec\alpha + \theta(\chi,\eta)\,R\tan\alpha - \rho\cos\alpha \tag{7}$$

where $\theta(\chi,\eta) = \dfrac{\cos\alpha}{R}(\chi - \eta\tan\alpha)$ (8)

and $\alpha$ is the helical angle of inclination relative to the diametral axis in the *x*-*y*-*z* space (Table 1) related to the tube length *L*, coil pitch *P* and number of helical turns $n_p$ as:

Published in: *Engineering Structures*, 85C, 234-248.
DOI: http://dx.doi.org/10.1016/j.engstruct.2014.12.033

$$P = 2\pi R \tan\alpha = \frac{L}{n_p} \tag{9}$$

The full curvilinear coordinate ranges along the helical coil are defined as:

$$0 \le \chi \le \left[ 2\pi R\cos\alpha + n_p \sqrt{P^2 + (2\pi R)^2} \right] \text{ and } 0 \le \eta \le \rho \tag{10}$$

where $\rho$ is the transverse 'width' of the coil strip:

$$\rho = \frac{2\pi RP}{\sqrt{P^2 + (2\pi R)^2}} \tag{11}$$

The present study requires the *inverse* of this transformation, namely:

$$\eta(x, y, z) = \left( z + \rho\cos\alpha - R\tan^{-1}\left(\frac{y}{x}\right)\tan\alpha \right)\cos\alpha \tag{12}$$

$$\chi(x, y, z) = \frac{R}{\cos\alpha}\tan^{-1}\left(\frac{y}{x}\right) + \eta\tan\alpha \tag{13}$$

This inverse transformation requires the following adjustment due to the fact that *tan*$^{-1}$ is a multi-valued function (*ceil* denotes rounded upwards to the nearest integer):

$$\left.\begin{aligned} \eta &= \eta - (n-1)\rho \\ \chi &= \chi + (n-1)\sqrt{(2\pi R)^2 - \rho^2} \end{aligned}\right\} \text{ if } n > 1 \text{ where } n = \left\lceil \frac{\eta}{\rho} \right\rceil = ceil\left(\frac{\eta}{\rho}\right) \tag{14}$$

Applying this transformation to the data effectively 'unwinds' the spiral coil and allows the weld imperfection to be viewed as a single continuous feature along the $\chi$ coordinate, illustrated in Fig. 12 for the spiral welded specimens T2 and T12, and thus ideally suited for an algebraic characterisation. A girth weld shows up as a feature inclined at $\alpha$ in the $\chi$-$\eta$ plane, while a coil weld appears as a feature located at a constant $\chi$ perpendicular to the strip.

Published in: *Engineering Structures*, 85C, 234-248.
DOI: http://dx.doi.org/10.1016/j.engstruct.2014.12.033

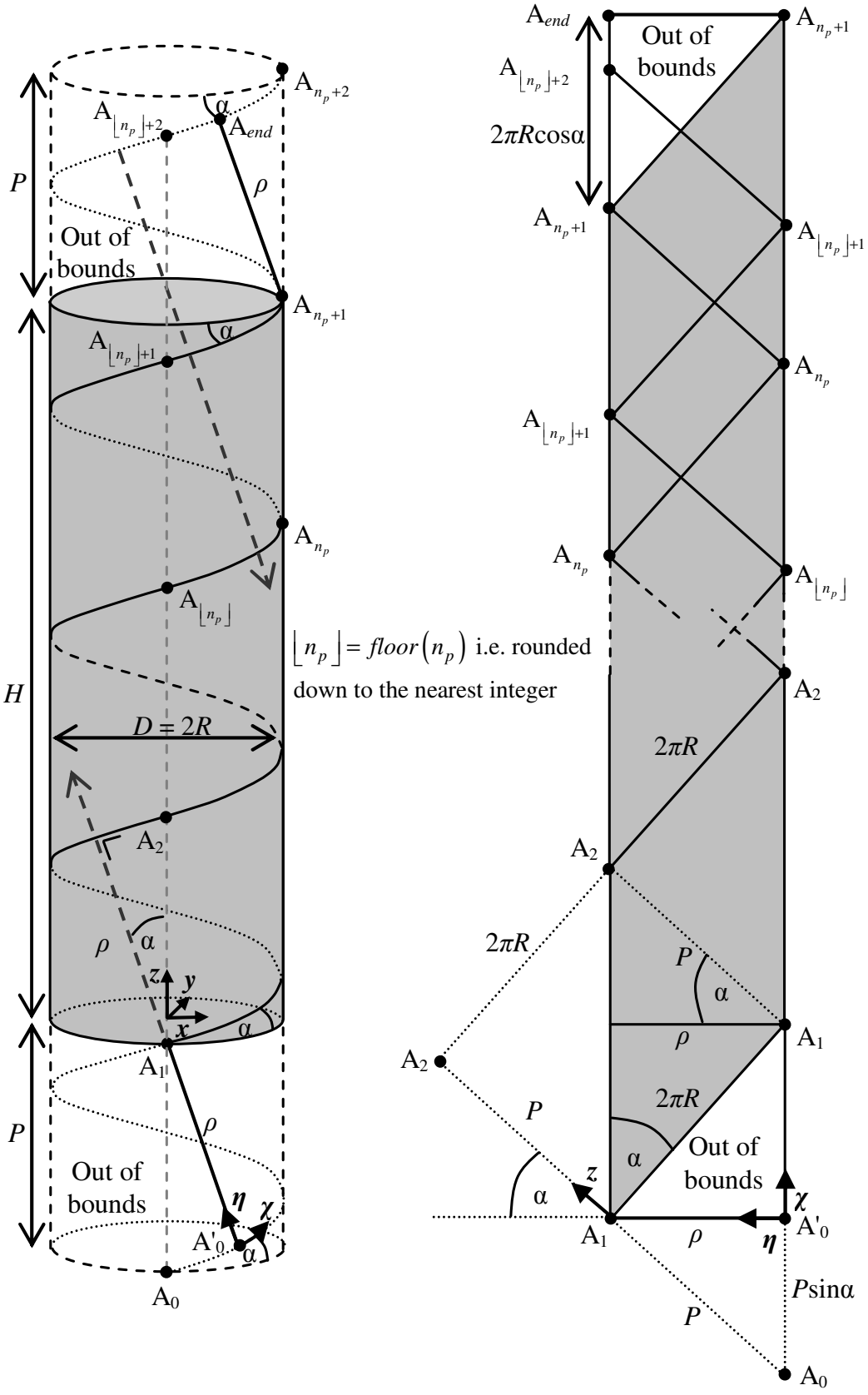


Fig. 11 – Conformal mapping of imperfections defined in a cylindrical coordinate system to a curvilinear coordinate system following the spiral strip (after [75])

Published in: *Engineering Structures*, 85C, 234-248.
DOI: http://dx.doi.org/10.1016/j.engstruct.2014.12.033

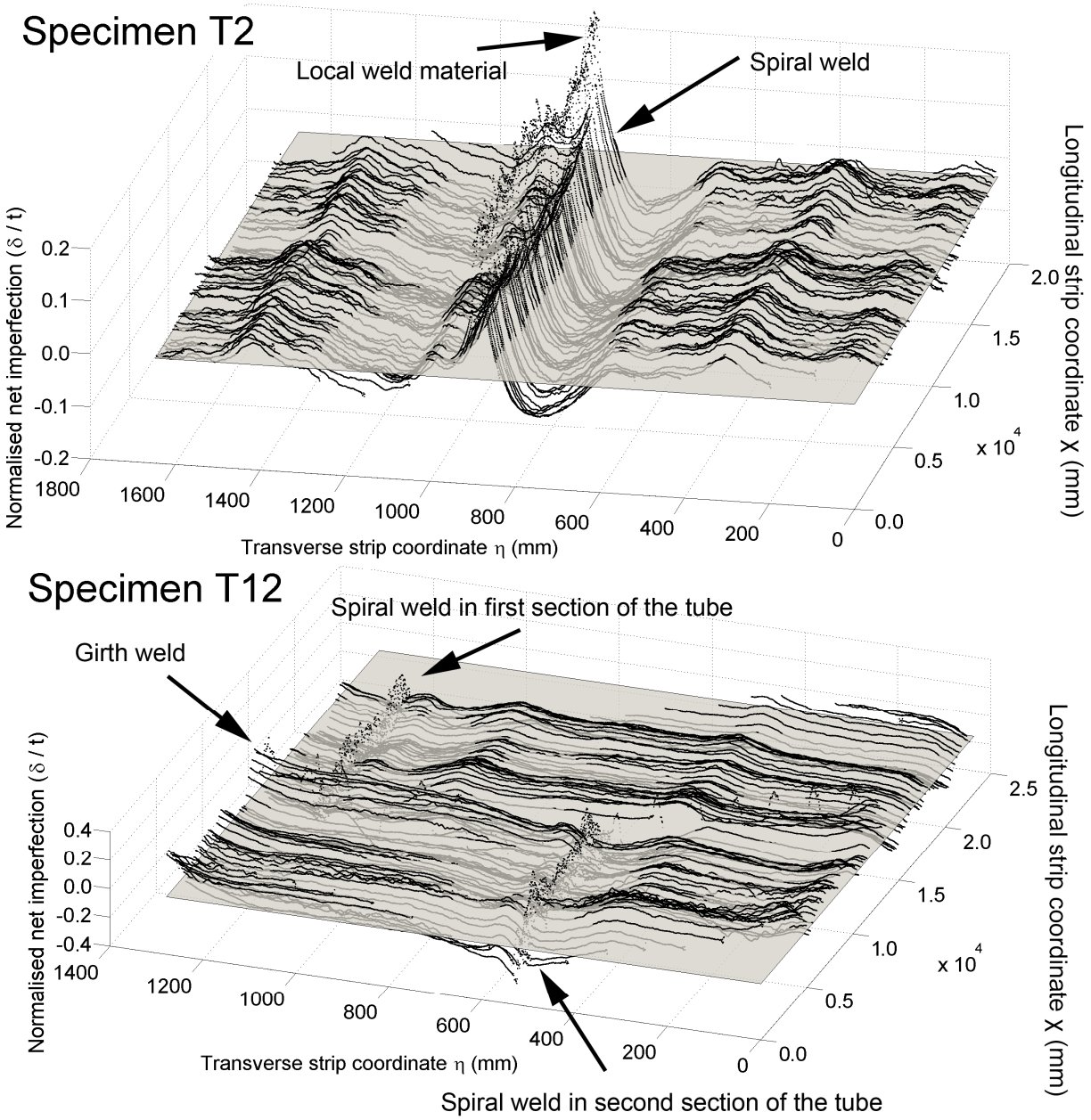


Fig. 12 – Surveyed net 'raw' deviations of spiral welded specimens T2 and T12 transformed to the helical $\chi$-$\eta$ plane

After having been 'cleaned' as before to remove the influence of the local weld material (Fig. 4), the imperfection data of each spiral welded tube specimen was transformed to the helical plane using Eqs 12 to 14 and subject to a corresponding 2D spline fitting procedure using the Matlab *griddata* command. This established an interpolated 'imperfection surface' defined on a uniformly-spaced $\chi$-$\eta$ grid which was then analysed at every individual $\eta$ coordinate with a traditional 1D full-wave Fourier series along the $\chi$ coordinate (Eq. 15). Up to $k = 10$ Fourier coefficients $a_k(\eta)$ and $b_k(\eta)$

Published in: *Engineering Structures*, 85C, 234-248.
DOI: http://dx.doi.org/10.1016/j.engstruct.2014.12.033

were extracted in this way for each relevant specimen (e.g. T4 in Fig. 13a), with the distributions across the strip as of yet not suggesting any discernible pattern.

$$w(\chi,\eta)=\sum_{k=0}^{K}\left(a_k(\eta)\cos\left(2\pi k\frac{\chi}{\chi_{\max}}\right)+b_k(\eta)\sin\left(2\pi k\frac{\chi}{\chi_{\max}}\right)\right) \tag{15}$$

where $\chi_{\max}=n_p\sqrt{P^2+(2\pi R)^2}$

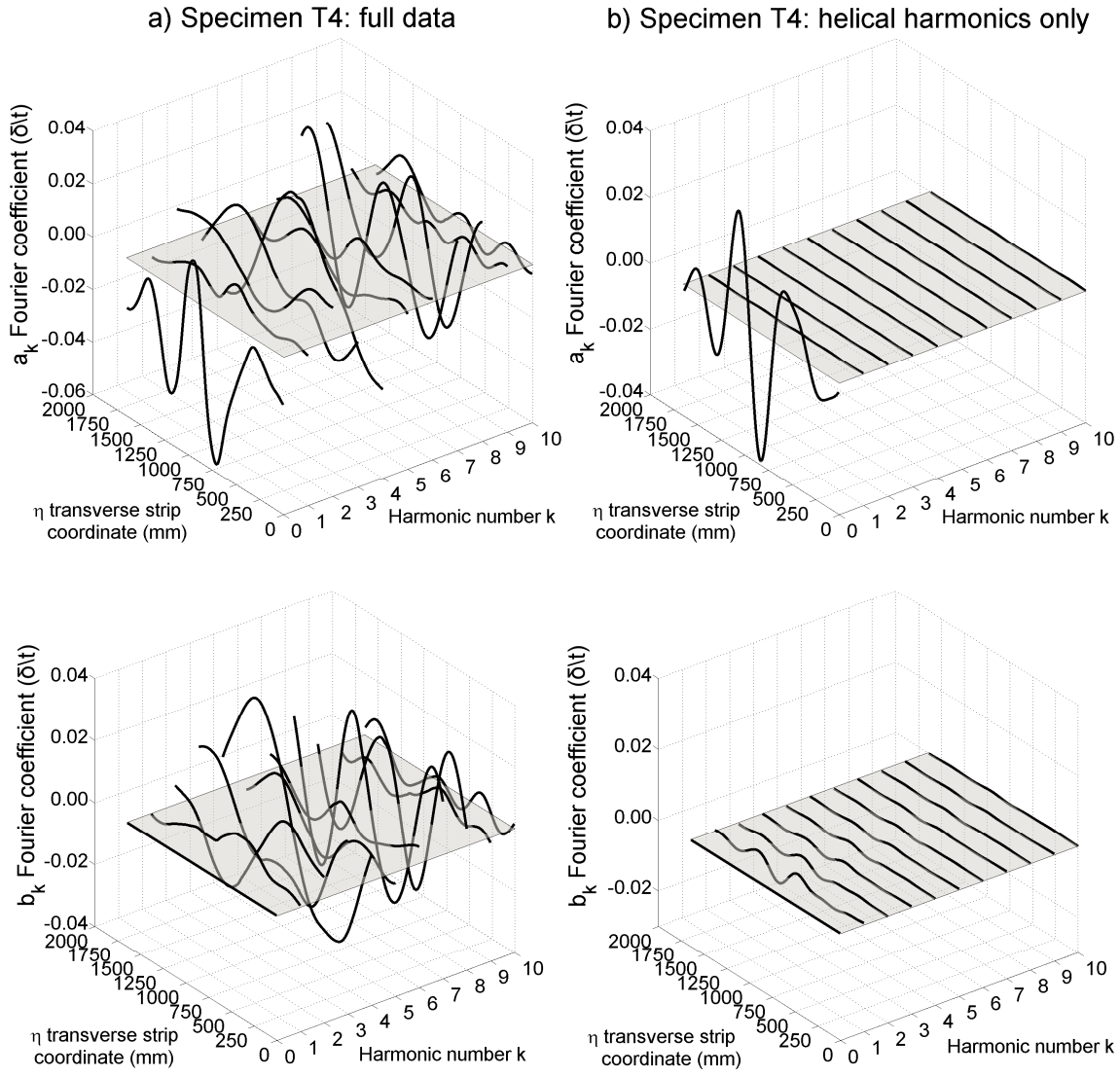


Fig. 13 – Distribution of the $a_k$ and $b_k$ Fourier coefficients (amplitudes in units of $\delta/t$) up to $k$ = 10 with $\eta$ in the helical plane for the transformed a) 'full' data and b) 'helical' harmonics only

It is important to appreciate that the aim of the mapping function was to be able to better study the effects of the spiral weld imperfection, but the data that was transformed clearly contains contributions from the full harmonic spectrum identified

Published in: *Engineering Structures*, 85C, 234-248.
DOI: http://dx.doi.org/10.1016/j.engstruct.2014.12.033

in Fig. 7 including 'low' harmonics which relate to global sagging and ovalisation etc. as well as 'high' harmonics which relate to miscellaneous local indentations (Fig. 6). To isolate the contributions of the spiral welding process from the full imperfection data, a 'filtered' imperfection surface was reconstituted in the $x$-$y$-$z$ space using *only* the 'helical' harmonics $(m,n) \approx ([n \times n_p],n)$ identified in Fig. 9. This reduced surface was then mapped onto the $\chi$-$\eta$ plane and subject to a 1D Fourier analysis (Eq. 14) in the same manner as above. The distributions of resulting Fourier coefficients $a_k(\eta)$ and $b_k(\eta)$ for a typical specimen (Fig. 13b) show that the contributions from every single coefficient except $a_0(\eta)$ have for practical purposes vanished as intended, with the distribution of $a_0(\eta)$ across the strip following a well-defined pattern that closely resembles the measured surface (Fig. 12 top) and is not unlike other characterisations of weld imperfections (e.g. Eq. 3). This was found to be the case for every spiral welded tube specimen.

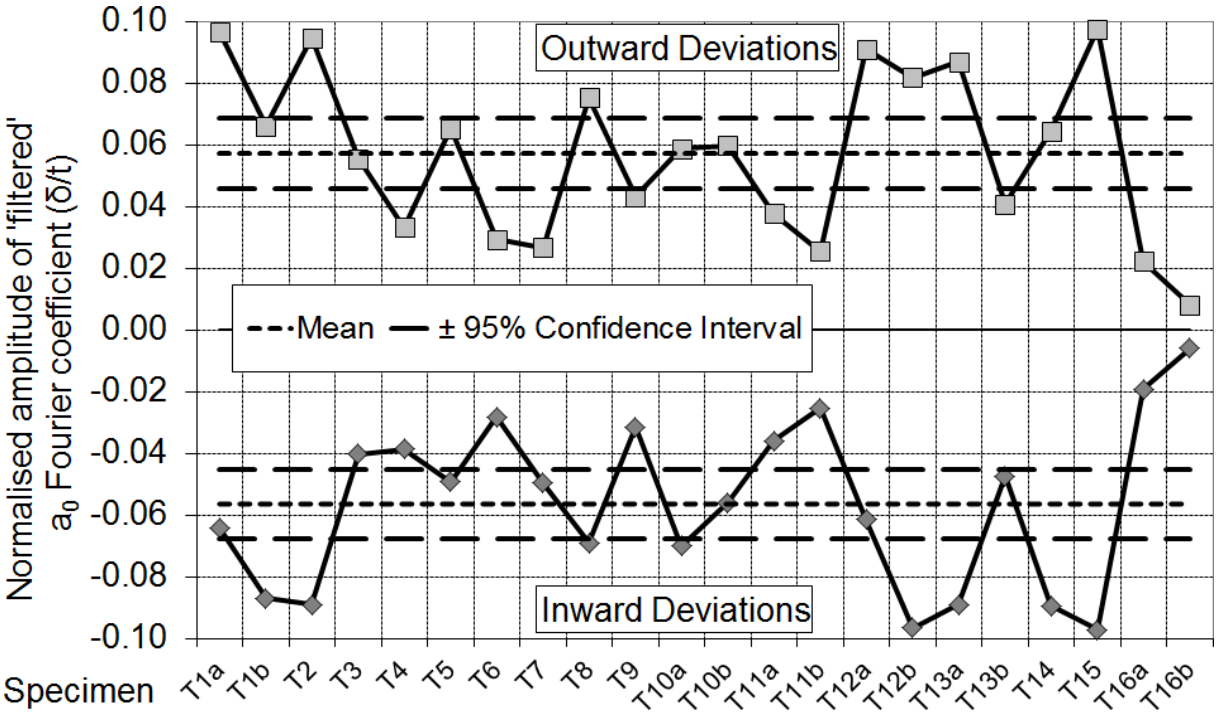


Fig. 14 – Peak filtered outward and inward deviations for the filtered $a_0(\eta)$ Fourier coefficient for each spiral welded tube specimen

The 1D Fourier analysis of the filtered imperfection surfaces was thus repeated for each one of the spiral welded tube specimens. Specimens containing a girth weld (T1, T10, T11, T12, T13 and T16; Table 1) were divided into two separate data sets (e.g.

T1a and T1b etc.), one for each part of the tube, and the analyses were performed on each part individually. The peak outward and inward deviations of the filtered $a_0(\eta)$ exhibit very modest means of $0.057t$ (CV = 47.5%) and $-0.056t$ (CV = 47.9%) respectively (Fig. 14) with rather narrow 95% Confidence Intervals (with a sample size of $n$ = 22), suggesting that the amplitude of the imperfection associated with spiral welding is very uniform for tubes in this $D/t$ range.

The extracted form of $a_0(\eta)$ lends itself reasonably well to an algebraic characterisation in terms of the transverse strip coordinate $\eta$ (Fig. 13b). For convenience, the data was adjusted to scale the peak inward deviation to -1 and to centre it at a normalised transverse strip coordinate $\bar{\eta} = \eta / \rho = 0$ (Fig. 15), where $\rho$ is the transverse strip width (Eq. 11). There is a periodic boundary condition at $\bar{\eta} = \pm$½. A simple one-part characterisation was attempted first:

$$w(\bar{\eta}) = \delta \cos(a\pi\bar{\eta}) \exp\left(-b|\bar{\eta}|^c\right) \tag{16}$$

where $\delta$ is the normalised imperfection amplitude (equal here to -1). The constants $a$, $b$ and $c$ were determined by a least-squares fitting procedure (using the Excel SOLVER functionality) which aimed to *maximise* the mean coefficient of determination $r^2$ of the fitted function (Eq. 16) to the computed distributions of $a_0(\eta)$ for the full set of spiral welded specimen components simultaneously. The $r^2$ coefficient is defined as:

$$r^2 = 1 - \frac{SS_{err}}{SS_{tot}} \text{ where } SS_{err} = \sum_{i=1}^{N} (y_i - f_i)^2 \text{ and } SS_{tot} = \sum_{i=1}^{N} (y_i - \bar{y})^2 \tag{17}$$

where $y_i$ and $f_i$ are the $i$-th measured data point and its fitted (predicted) value respectively out of a total of $N$ data points while $\bar{y}$ is the mean of all measured values. Though strictly valid for linear regressions (since Eq. 17 can become negative for poorly-fitting nonlinear functions), the $r^2$ coefficient is cautiously accepted in practice as a reasonable 'goodness of fit' measure in nonlinear regressions because of its simplicity [76].

The constants in Eq. 16 were found to be $a$ = 6.7, $b$ = 34 and $c$ = 2 corresponding to a reasonable mean $r^2$ coefficient of 0.45 (CV = 36.5%). A two-part characterisation which recognises that the distribution of $a_0$ is not fully symmetric about $\bar{\eta} = 0$ was also attempted:

Published in: *Engineering Structures*, 85C, 234-248.
DOI: http://dx.doi.org/10.1016/j.engstruct.2014.12.033

$$w(\bar{\eta}) = \begin{cases} \delta \cos(a_{-}\pi\bar{\eta}) \exp\left(-b_{-}|\bar{\eta}|^{c_{-}}\right) & \bar{\eta} < 0 \\ \delta \cos(a_{+}\pi\bar{\eta}) \exp\left(-b_{+}|\bar{\eta}|^{c_{+}}\right) & \bar{\eta} \geq 0 \end{cases} \quad (18)$$

where, using a similar fitting criterion, the respective constants were found to be $a_{-}$ = 6.6, $b_{-}$ = 24, $c_{-}$ = 2, $a_{+}$ = 5.7, $b_{+}$ = 9 and $c_{+}$ = 1.2 corresponding to a distinctly higher mean $r^2$ of 0.58 (CV = 31.2%). Both Eqs 17 and 18 decay to less than $1\times10^{-5}t$ towards the strip edges $\bar{\eta}$ = ±½ at the imperfection amplitudes suggested by Fig. 14. The relatively low mean $r^2$ coefficients are a reflection of the still considerable scatter in the distributions of $a_0(\eta)$ across the full range of specimens (Fig. 15).

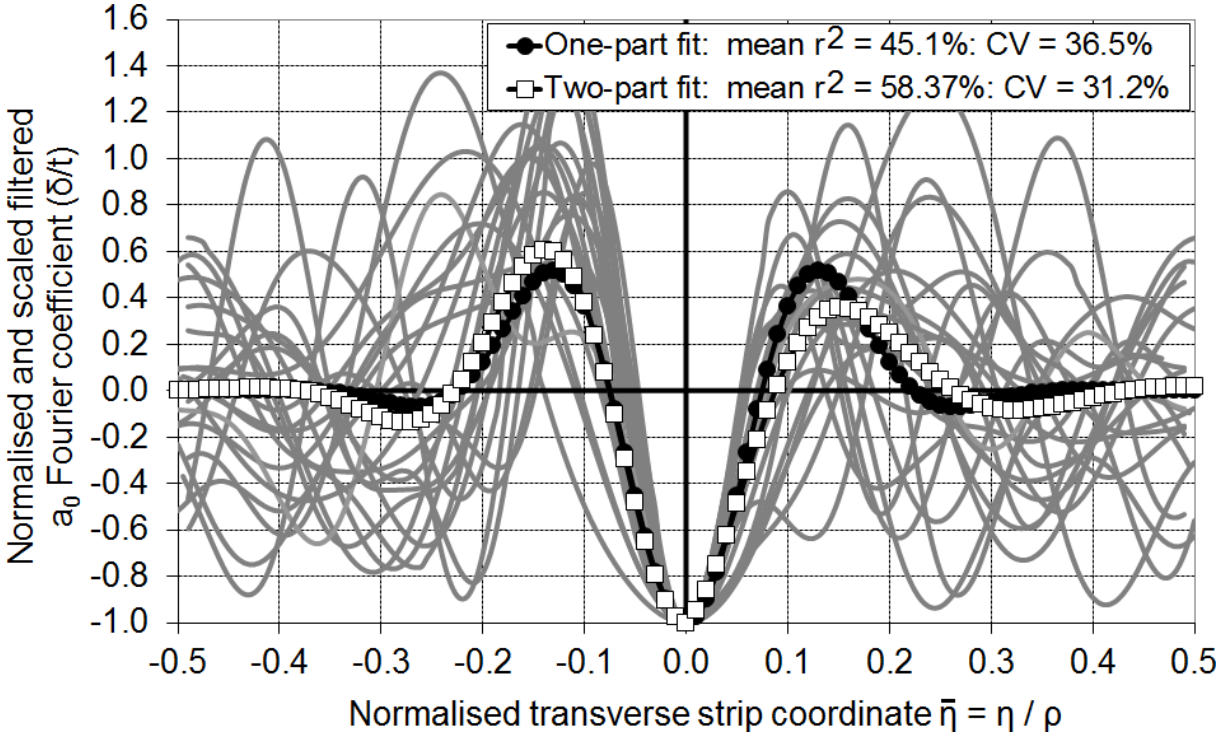


Fig. 15 – Least-squares characterisation of spiral weld imperfection in the helical plane (amplitudes have been scaled to give a peak inwards deviation of negative unity; grey lines represent the 'as measured' $a_0(\eta)$ distributions e.g. Fig. 13b)

The final imperfection feature, a coil weld, is rather more difficult to characterise in the above manner because it is quite localised, spanning only a small portion of the surface area of a typical specimen and consequently not being covered with as high a resolution of sampling points as the other features. Furthermore, it leaves no obvious 'signal' on the harmonic spectrum (Fig. 7) and is therefore impossible to isolate from the remainder of the geometric data. Nonetheless, a typical coil weld appears to be

Published in: *Engineering Structures*, 85C, 234-248.
DOI: http://dx.doi.org/10.1016/j.engstruct.2014.12.033

accompanied by its own local depression that is orthogonal to the spiral weld feature (Fig. 16). Approximate normalised profiles of the coil weld depressions for specimens T1, T5, T10, T13 and T15 (but not T14 as its coil weld was found to lie too close to an end boundary to yield a useful profile; Table 1) may be obtained by taking the mean deviation at every $\chi$ coordinate (effectively the $a_0(\chi)$ coefficient of a 1D Fourier series in terms of $\eta$ instead of $\chi$; Eq. 15) and plotting this against $\chi$ normalised by the linear meridional bending half-wavelength $\lambda$ (Eq. 4). Shown in Fig. 17, these profiles display significant variation due to interference from other modal forms, though each one appears to exhibit a distinct local depression that appears to be captured reasonably well by a proposed modified version of the Rotter and Teng [38] Type 'A' weld (Eq. 19). This form is adapted here to the $\chi$-$\eta$ plane and to take account of the possible influence of the helical angle $\alpha$ on the local radius of curvature and thus the linear bending half-wavelength $\lambda(\alpha)$. It is thought that this characterisation may be sufficiently realistic to define a coil weld in the helical $\chi$-$\eta$ plane where this is deemed necessary, for example for numerical modelling purposes.

$$w(\chi) = \delta e^{-\pi|\chi-\chi_w|/\lambda(\alpha)} \left( \cos\frac{\pi}{\lambda(\alpha)}|\chi-\chi_w| + \sin\frac{\pi}{\lambda(\alpha)}|\chi-\chi_w| \right) \tag{19}$$

where $\lambda(\alpha) = \dfrac{\pi\sqrt{rt\sec\alpha}}{\sqrt[4]{3\left(1-\nu^2\right)}}$ is the modified linear bending half-wavelength

Published in: *Engineering Structures*, 85C, 234-248.
DOI: http://dx.doi.org/10.1016/j.engstruct.2014.12.033

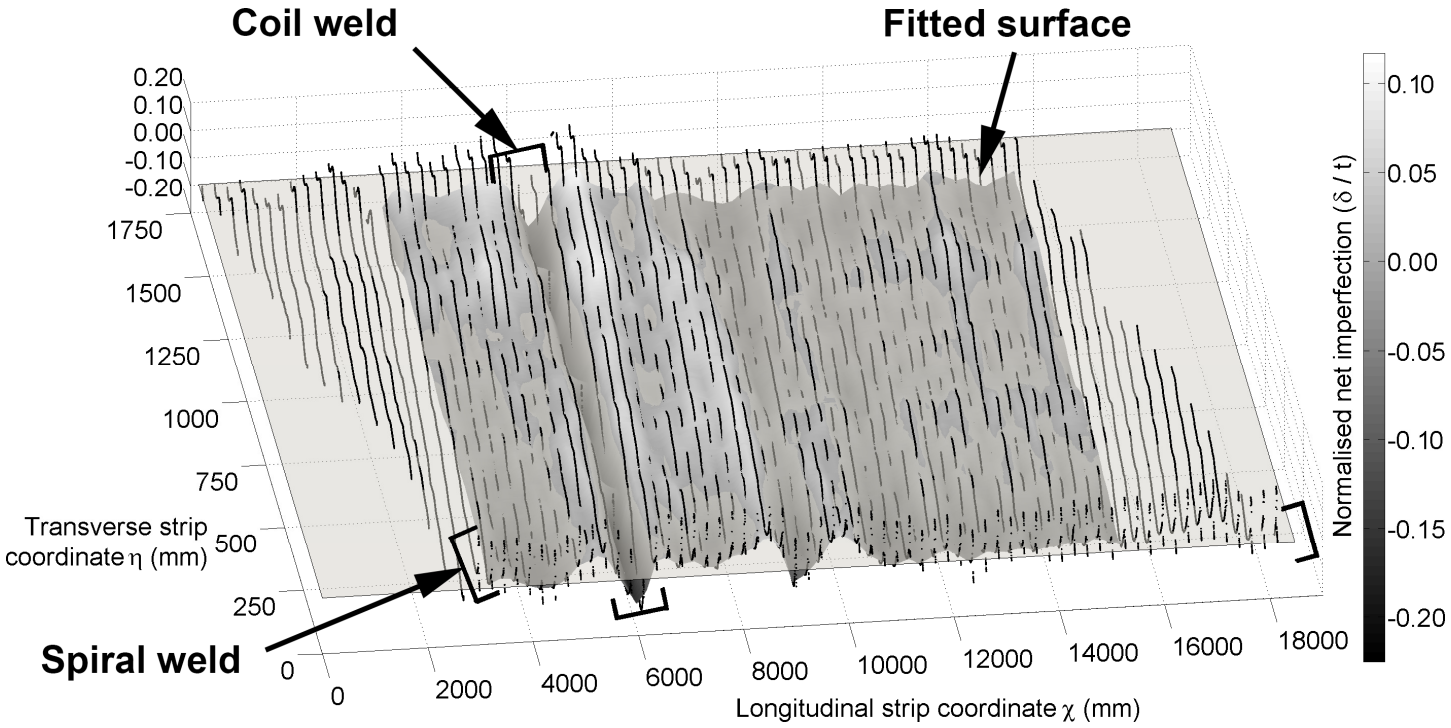


Fig. 16 – Illustration of the coil weld of specimen T5 in the helical plane

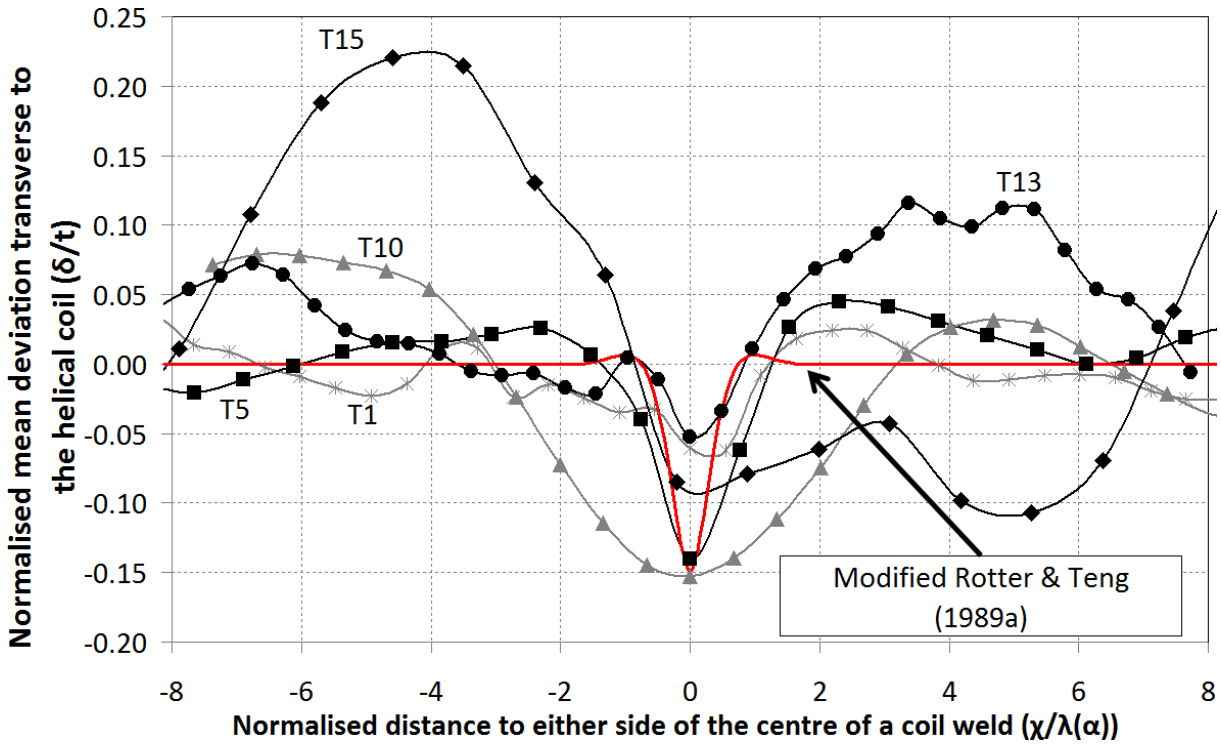


Fig. 17 – Coil weld profiles for specimens T1, T5, T10, T13 and T15 compared with a modified version of the Rotter and Teng [38] Type 'A' weld depression (shown for an imperfection amplitude of 0.15*t*)

Published in: *Engineering Structures*, 85C, 234-248.
DOI: http://dx.doi.org/10.1016/j.engstruct.2014.12.033

## Conclusions

This paper has presented a detailed summary and analysis of the results of careful laser surveys of the initial outside surface imperfections of sixteen spiral welded carbon steel tubes with *D*/*t* ratios in the range 67 to 119. The specimens are representative of those widely used in practice in deep retaining walls. Two longitudinally-welded tubes were additionally employed as 'control' specimens. The data was collected at the Delft University of Technology and the Karlsruhe Institute of Technology.

The spiral welded tube specimens were found to exhibit very distinct patterns of systematic imperfections caused by the unique manufacturing process in addition to a number of miscellaneous features, some of which were most likely caused by accidental local impact. The magnitudes of the systematic imperfection features were found to satisfy at least the requirements of Fabrication Quality Class C 'Normal' of the European Standard on Metal Shells EN 1993-1-6 for cylinders with corresponding *D*/*t* ratios.

An attempt was made to characterise all systematic imperfection features algebraically using 1D and 2D harmonic analyses and minimum least squares curve fitting. These features included spiral welds, girth welds and coil welds. Though the data exhibits a lot of variation and scatter, some generalisations could be made and the results presented here are thought to be the first of their kind. The structural consequences of these imperfections for tubes within this *D*/*t* range fall outside the scope of this particular study and will be considered at a later stage.

## Acknowledgements

This work was carried out as part of the EU RFCS Combitube research project funded by the European Commission, grant contract RFSR-CT-2011-00034.

## References

[1] CUR (2013). "Handbook Quay Walls 2nd Edition - Publication N. C211E", *Centre for Civil Engineering Research and Codes (CUR)*, Gouda, Holland.

[2] EN 1993-1-1 (2003). "Eurocode 3: Design of steel structures - Part 1.1: General rules and rules for building." *Comité Européen de Normalisation*, Brussels.

[3] EN 1993-1-6 (2007). "Eurocode 3: Design of steel structures - Part 1.6: Strength and stability of shell structures." *Comité Européen de Normalisation*, Brussels.

[4] Combitube (2010). "Bending resistance of steel tubes in CombiWalls." *RFCS Research Proposal Form*, Research Fund for Coal and Steel, European Commission.

[5] Arbocz J. & Babcock C.D.Jr. (1969). "The effect of general imperfections on the buckling of cylindrical shells." *ASME Journal of Applied Mechanics*, 36, 28-38.

[6] Arbocz J. & Babcock C.D.Jr. (1976). "Prediction of buckling loads based on experimentally measured initial imperfections." in *Buckling of Structures*, Ed. B. Budiansky, Proc. IUTAM Symposium, Harvard University, June 1974, Springer, 291-311.

[7] Arbocz J. (1974). "The effect of initial imperfections on shell stability." in *Thin Shell Structures*, Ed. Y.C. Fung and E.E. Sechler, Prentice Hall, 205-246.

[8] Arbocz J. & Williams J.G. (1977). "Imperfection surveys on a 10-ft-diameter shell structure." *AIAA Journal*, 15(7), 949-956.

[9] Singer J., Arbocz J. & Babcock C.D.Jr. (1979). "Buckling of imperfection stiffened cylindrical shells under axial compression." *AIAA Journal*, 9(1), 68-75.

[10] Arbocz J. & Abramovich H. (1979). "The Initial Imperfection Data Bank at the Delft University of Technology - part I." *Report LR-290*, Delft University of Technology, the Netherlands.

[11] Arbocz J. (1982). "The Imperfection Data Bank, a means to obtain realistic buckling loads." in *Buckling of Shells*, Ed. E. Ramm, Springer Verlag, Berlin, 535-567.

[12] Singer J. (1982). "The status of experimental buckling investigations of shells." in *Buckling of Shells*, Ed. E. Ramm, Springer Verlag, Berlin, 501-533.

[13] Singer J., Abramovich H. & Yaffe R. (1978). "Initial imperfection measurements of integrally stringer-stiffened shells." *TAE Report n. 330*, Technion, Haifa, Israel.

[14] Singer J. & Abramovich H. (1995). "The development of shell imperfection measurement techniques." *Thin-Walled Structures*, 23, 379-398.

[15] Singer J., Weller T. & Abramovich H. (1991). "The influence of initial imperfections on the buckling of stiffened cylindrical shells under combined loading." in *Buckling of shell structures on land, in the sea and in the air*, Ed. J.F. Jullien, Elsevier Applied Science, London, 1-10.

[16] Singer J., Arbocz J. & Weller T. (2002). "Buckling experiments: Experimental methods in buckling of thin-walled structures" 2 volumes, *Wiley-VCH Verlag*.

[17] Sebek R.W.L. (1981). "Imperfection surveys and data reduction of ARIANE Interstages I/II and II/III" *Ir. Thesis*, Delft University of Technology.

[18] Arbocz J. & Hol M.A.M. (1991). "Collapse of axially compressed cylindrical shells with random imperfections." *AIAA Journal*, 29(12), 2247-2256.

[19] Esong I.E., Elghazouli A.Y. & Chryssanthopoulos (1998). "Measurement techniques for buckling sensitive composite shells." *Strain*, 34(1), 11-17.

[20] Elghazouli A.Y., Chryssanthopoulos & Esong I.E. (1999). “Buckling of woven GFRP cylinders under concentric and eccentric compression.” *Composite Structures*, 45, 13-27.

[21] Chryssanthopoulos M.K., Elghazouli A.Y. & Esong I.E. (1999). “Compression tests on anti-symmetric two-ply GFRP cylinders.” *Composites Part B: Engineering*, 30, 335-350.

[22] Chryssanthopoulos M.K., Elghazouli A.Y. & Esong I.E. (2000). "Validation of FE models for buckling analysis of woven GFRP shells." *Composite Structures*, 49, 355-367.

[23] Odland J. & Didriksen T. (1977a). "Buckling experiments with spherical shell segments - Part I - test equipment." *Det Norske Veritas*, Report N. 77-442.

[24] Odland J. & Didriksen T. (1977b). "Buckling experiments with spherical shell segments - Part II - testing and measurement." *Det Norske Veritas*, Report N. 77-532.

[25] Rotter J.M., Coleman R., Ding X.L. & Teng J.G. (1992). "The measurement of imperfections in cylindrical silos for buckling strength assessment." *Proc. 4th Int. Conf. on Bulk Materials Storage, Handing and Transportation*, IE Australia, Wollongong, 473-479.

[26] Clarke M.J. & Rotter J.M. (1988). "A technique for the measurement of imperfections in prototype silos and tanks." *Research Report R565*, School of Civil and Mining Engineering, University of Sydney, Australia.

[27] Coleman R., Ding X.L. & Rotter J.M. (1992). "The measurement of imperfections in full-scale steel silos." *Proc. 4th Int. Conf. on Bulk Materials Storage, Handing and Transportation*, IE Australia, Wollongong, 467-472.

[28] Ding X. (1992). "Precise engineering surveying: application to the measurement of lare scale engineering silos." *PhD Thesis*, School of Civil and Mining Engineering, University of Sydney, Australia.

[29] Ding X., Coleman R. & Rotter J.M. (1996a). "Surface profiling system for measurement of engineering structures." *ASCE Journal of Surveying Engineering*, 122(1), 3-13.

[30] Ding X., Coleman R. & Rotter J.M. (1996b). "Technique for precise measurement of large-scale silos and tanks." *ASCE Journal of Surveying Engineering*, 122(1), 14-25.

[31] Berry P.A., Bridge R.Q. & Rotter J.M. (1997). "Experiments on the buckling of axially compressed fabricated steel cylinders with axisymmetric imperfections." *Proc. Int. Conf. on Carrying Capacity of Steel Shell Structures*, Brno, 1-3 October, 347-353.

[32] Berry P.A., Bridge R.Q. & Rotter J.M. (1999). "Characterising asymmetry of the initial imperfections in steel silos." in *Mechanics of Structures and Materials*, Eds M.A. Bradford, R.Q. Bridge & S.F. Foster, Balkema, Rotterdam, 233-238.

[33] Berry P.A., Rotter J.M. & Bridge R.Q. (2000). "Compression tests on cylinders with circumferential weld depressions." *ASCE Journal of Engineering Mechanics*, 126(4), 405-413.

[34] Pircher M., Berry P.A., Ding X. & Bridge R.Q. (2001). "The shape of circumferential weld-induced imperfections in thin-walled steel silos and tanks." *Thin-Walled Structures*, 39, 999-1014.

[35] Teng J.G., Lin X., Rotter J.M. & Ding X.L. (2005). "Analysis of geometric imperfections in full-scale welded silos." *Engineering Structures*, 27, 938-950.

[36] Koiter W.T. (1963). "The effect of axisymmetric imperfections on the buckling of cylindrical shells under axial compression." *Proc. Koniklijke Nederlandse Akademie von Wetenschappen*, Series B, 66(5), 265-279.

[37] Hutchinson J. (1965). "Axial buckling of pressurised imperfect cylindrical shells." *AIAA Journal*, 3(8), 1461-1466.

[38] Rotter J.M. & Teng J.G. (1989a). "Elastic stability of cylindrical shells with weld depressions." *ASCE Journal of Structural Engineering*, 115(5), 1244-1263.

[39] Teng J.G. & Rotter J.M. (1992). "Buckling of pressurized axisymmetrically imperfect cylinders." *ASCE Journal of Engineering Mechanics*, 118(2), 229-247,

[40] Teng J.G., Zhao Y. & Lam L. (2001). "Techniques for buckling experiments on steel silo transition junctions." *Thin-Walled Structures*, 39, 685-707.

[41] Zhao Y. & Teng J.G. (2001). "Buckling experiments on cone-cylinder intersections under internal pressure." *ASCE Journal of Engineering Mechanics*, 127(12), 1231-1239.

[42] Zhao Y. & Teng J.G. (2004). "Buckling experiments on steel silo transition junctions. I: Experimental results." *Journal of Constructional Steel Research*, 60, 1783-1801.

[43] Hornung U. & Saal H. (2002). "Buckling loads of tank shells with imperfections." *International Journal of Nonlinear Mechanics*, 37, 605-621.

[44] Knödel P., Ummenhofer T. & Schulz U. (1995). "On the modelling of different types of imperfections in silo shells." *Thin-Walled Structures*, 23, 283-293.

[45] Knödel P. & Ummenhofer T. (1996). "Substitute imperfections for the prediction of buckling loads in shell design." *Proc. Intl. Workshop on Imperfections in Metal Silos: Measurement, Characterisation and Strength Analysis*, CA-Silo, Lyon, France, 87-102.

[46] Ummenhofer T. & Knödel P. (1996). "Typical imperfections of steel silo shells in civil engineering." *Proc. Intl. Workshop on Imperfections in Metal Silos: Measurement, Characterisation and Strength Analysis*, CA-Silo, Lyon, France, 103-118.

[47] Rotter J.M. (1996). "Elastic plastic buckling and collapse in internally pressurised axially compressed silo cylinders with measured axisymmetric imperfections: interactions between imperfections, residual stresses and collapse." *Proc. Intl. Workshop on Imperfections in Metal Silos: Measurement, Characterisation and Strength Analysis*, CA-Silo, Lyon, France, 119-140.

[48] Rotter J.M. & Schmidt H. (2008). "Geometric tolerances and imperfections." in *Stability of Steel Shells: European Design Recommendations: Fifth Edition*, European Convention for Constructional Steelwork, Brussels, 69-82.

[49] Esslinger M. (1973). "Buckling loads of steel metal silos with overlapping circumferential seams." *Deutscher Forschungs- und Versuchsanstalt für Luft- und Raumfahrt*, Report DLR-FB 73-36, Braunschweig.

[50] Rotter J.M. & Teng J.G. (1989b). "Elastic stability of lap-jointed cylinders." *ASCE Journal of Structural Engineering*, 115(3), 683-697.

[51] Holst J.M.F.G., Rotter J.M. & Calladine C.R. (1999). "Imperfections in cylindrical shells resulting from fabrication misfits." *ASCE Journal of Engineering Mechanics*, 125(4), 410-418.

[52] Holst J.M.F.G., Rotter J.M. & Calladine C.R. (2000). "Imperfections and buckling in cylindrical shells with consistent residual stresses." *Journal of Constructional Steel Research*, 54, 265-282.

[53] Holst J.M.F.G. & Rotter J.M. (2005). "Axially compressed cylindrical shells with local settlement." *Thin-Walled Structures*, 43, 811-825.

[54] Hübner A., Albiez M., Kohler D. & Saal H. (2007). "Buckling of long steel cylindrical shells subject to external pressure." *Thin-Walled Structures*, 45, 1-7.

[55] Sadowski A.J. & Rotter J.M. (2013). "Exploration of novel geometric imperfection forms in buckling failures of thin-walled metal silos under eccentric discharge." *International Journal of Solids and Structures*, 50, 781-794.

[56] Mathworks (2013). "Matlab Release 2013a" *Mathworks*, Natick, MA, USA.

[57] Sadowski A.J., Rotter J.M., Reinke T. & Ummenhofer T. (2015). “Analysis of variance of tensile tests from spiral welded carbon steel tubes.” *Construction and Building Materials*, 75C, 208-212.

[58] Sensopart (2011). “FT50 RLA-40-F Distance sensor with high resolution and small light spot.” Accessed on 13/09/2014 from:

Published in: *Engineering Structures*, 85C, 234-248.
DOI: http://dx.doi.org/10.1016/j.engstruct.2014.12.033

http://www.sensopart.com/en/products/distance-sensors/distance-sensors/ft-50-rla-40-f-l4s.html

[59] van Es S.H.J., Gresnigt A.M., Kolstein M.H. & Bijlaard F.S.K. (2013). "Local buckling of spirally welded tubes - Analysis of imperfections and physical testing." *Proc. Int. Offshore and Polar Engineering Conference (ISOPE)*, Anchorage, Alaska.

[60] Mohr L.B. (1990). "Understanding significance testing." *Sage University Paper Series on Quantitative Applications in Social Sciences*, 07-073, Newbury Park, Sage.

[61] Leica (2012). "ScanStation C10 Datasheet." Accessed on 13/09/2014 from http:/www.leica-geosystems.de/de/Leica-ScanStation-C10_79411.htm

[62] Coppa A.P. (1966). "Measurements of initial geometric imperfections of cylindrical shells." *AIAA Journal*, 4(1), 172-177.

[63] Lin X. (2004). "Buckling of extensively welded steel cylindrical shells under axial compression." *PhD Thesis*, The Hong Kong Polytechnic University, Hong Kong, China.

[64] Agelidis N., Harding J.E. & Dowling P.J. (1982). "Buckling tests on stringer-stiffened cylinder models subject to load combination." *DNV Report N. 82-0298*, Det Norske Veritas, Norway.

[65] Chryssanthopoulos M.K., Baker M.J. & Dowling P.J. (1991). "Statistical analysis of imperfections in stiffened cylinders." *ASCE Journal of Structural Engineering*, 117(7), 1979-1997.

[66] Chryssanthopoulos M.K. & Poggi C. (1995). "Stochastic imperfection modelling in shell buckling studies." *Thin-Walled Structures*, 23, 179-200.

[67] Cederbaum G. & Arbocz J. (1996) "On the reliability of imperfection-sensitive long isotropic cylindrical shells." *Structural Safety*, 18(1), 1-9.

[68] Lin X. & Teng J.G. (2003). "Iterative Fourier decomposition of imperfection measurements at non-uniformly distributed sampling points." *Thin-Walled Structures*, 41, 901-924.

[69] EN 1090-2 (2008). "European Standard: Execution of steel structures and aluminium structures - Part 2: Technical requirements for steel structures." *Comité Européen de Normalisation*, Brussels.

[70] EN 10219-2 (2006). "European Standard: Cold formed welded structural hollow sections of non-alloy and fine grain steels - Part 2: Tolerances, dimensions and section properties." *Comité Européen de Normalisation*, Brussels.

[71] Tennyson R.C. & Muggeridge D.B. (1969). "Buckling of axisymmetric imperfect circular cylindrical shells under axial compression." *AIAA Journal*, 7, 2127-2131.

[72] Pircher M. & Bridge R.Q. (2001). "The influence of circumferential weld-induced imperfections on the buckling of silos and tanks." *Journal of Constructional Steel Research*, 57(5), 569-580.

[73] Hübner A., Teng J.G. & Saal H. (2006). "Buckling behaviour of large steel cylinders with patterned welds." *International Journal of Pressure Vessels and Piping*, 83, 13-26.

[74] Song C.Y., Teng J.G. & Rotter J.M. (2004). "Imperfection sensitivity of thin elastic cylindrical shells subject to partial axial compression." *International Journal of Solids and Structures*, 41, 7155-7180.

[75] Sadowski A.J. & Rotter J.M. (2014). "Modelling and behaviour of cylindrical shell structures with helical features." *Computers and Structures*, 133C, 90-102.

[76] Nagelkerge N.J.D. (1991). "A note on a general definition of the coefficient of determination." *Biometrika*, 78(3), 691-692.